International Geology Review
Vol. 51, No. 5, May 2009, 388–421

Geochronological and geochemical constraints on formation of the Tongling metal deposits, middle Yangtze metallogenic belt, east-central China

Jiancheng Xie[a,b], Xiaoyong Yang[a,c]*, Weidong Sun[a,c]*, Jianguo Du[d], Wei Xu[d], Libin Wu[d], Keyou Wang[d] and Xiaowei Du[a]

[a]*CAS Key Laboratory of Crust-Mantle Materials and Environments, School of Earth and Space Sciences, University of Science and Technology of China, Hefei 230026, China;* [b]*School of Resource and Environmental Sciences, Hefei University of Technology, Hefei 230009, China;* [c]*CAS Key Laboratory of Isotope Geochronology and Geochemistry, Guangzhou Institute of Geochemistry, Guangzhou 510640, China;* [d]*Anhui Academy of Geological Survey, Hefei 230001, China*

(*Accepted 22 December 2008*)

The Tongling district is one of the most important non-ferrous metal producers in China. The origin of Cu–Au deposits in the region is closely related to Late Mesozoic intermediate intrusions, which are mainly high-K calc-alkaline and shoshonitic series. Geochemical characteristics indicate that these granitic rocks are mixtures of more than two compositional end-members, i.e. mantle-derived melts and crust components incorporated through assimilation. Three important magmatic intrusions related to the Cu–Au deposits in the Tongling region – the Jiguanshi quartz monzodiorite, the Xishizishan quartz diorite and the Miaojia diorite porphyry – were selected for this study. Zircon U–Pb dating by LA ICP-MS yielded two groups of ages (~130–132 and 138–140 Ma) for these intrusions. Pyrite Re–Os age for the Xinqiao Cu–Fe–S deposit in the Tongling region is 126 ± 11 Ma. Trace elements of zircon grains show that the earlier Cu–Au mineralization event was associated with adakitic rocks characterized by high positive Ce anomalies, produced at an elevated oxygen fugacity range. In contrast, later iron-sulphur mineralization was closely related to low positive Ce anomalies, reflecting low oxygen fugacities. Considering that Pacific lithospheric subduction was the dominant factor that controlled major tectonic evolution in eastern China during the Early Cretaceous, the geochemical characteristics of these coeval ore-forming intermediate intrusive rocks in the Tongling district were likely the result of Pacific plate underflow.

Keywords: high-K calc-alkaline and shoshonite; Mesozoic intermediate intrusive rock; LA-ICP-MS geochronology; magma mixing; subduction of the Pacific plate; Tongling Cu-Au deposits

Introduction

The Tongling region of Anhui Province in central eastern China is an important ore district of the famous Lower and Middle Yangtze River metallogenic belt, and also

*Corresponding authors. Email: xyyang555@163.com; weidongsun@gig.ac.cn

ISSN 0020-6814 print/ISSN 1938-2839 online

DOI: 10.1080/00206810802712004
http://www.informaworld.com

a good example of skarn deposits in China (Chang *et al.* 1991; Zhai *et al.* 1992, 1996; Pan and Dong 1999; Xu and Lin 2000; Xu and Zhou 2001; Deng *et al.* 2002). Many researchers have proposed that the metal deposits are closely related to the Mesozoic intrusive rocks in the region (Weng 1920; Guo 1982; Chang *et al.* 1991; Zhai *et al.* 1992; Xing and Xu 1995, 1996, 1999; Li *et al.* 1998; Tang *et al.* 1998; Xing 1998; Zhou and Li 2000; Wu *et al.* 2000, 2003; Wang *et al.* 2003a). Therefore, knowledge of the formation and ages of these intrusive rocks is essential for understanding the formation of these deposits. The petrogenesis of these intrusive rocks in the Tongling region, however, has been a matter of much debate (Yang and Lin 1988; Mao *et al.* 1990; Xing and Xu 1996; Du and Li 1997; Chen and Jahn 1998; Tang *et al.* 1998; Xing 1998; Wu *et al.* 2000; Deng and Wu 2001; Zhang *et al.* 2001a, b; Wang *et al.* 2003a, b, 2004b; Xie *et al.* 2008). At least three models have been suggested for the formation of Tongling intrusive rocks: (1) the mixing of mantle-derived and crust-derived magmas, or assimilation and fractional crystallization process of a mantle-derived magma, with major contributions from an ancient crustal component (Chen *et al.* 1985, 1993; Chen and Jahn 1998; Wu *et al.* 2000; Deng and Wu 2001); (2) partial melting of lower crust materials in the Yangtze continental block (Yang and Lin 1988; Du and Li 1997; Zhang *et al.* 2001a, b; Wang *et al.* 2004c); (3) rocks with $SiO_2 \leqslant 55\%$ were produced by crystallization of basaltic magmas derived from an enriched mantle, with limited assimilation of lower crustal materials; whereas rocks with $SiO_2 > 55\%$ were generated by mixing of mantle-derived basaltic magmas and adakite-like magmas derived from the melting of basaltic lower crust due to heating of underplating shoshonitic magmas (Wang *et al.* 2003a,b).

Metal deposits in the Tongling region have long been studied using isotope geochronological methods (Chen *et al.* 1985, 1993; Zhou *et al.* 1987). Most of the early data, however, were whole rock K–Ar and Rb–Sr isochron ages, which usually represent cooling ages of high temperature intrusive rocks (Chen *et al.* 1985, 1993; Zhou *et al.* 1987; Xing and Xu 1996; Wu *et al.* 1996, 2000). In this study, we obtain zircon geochemical and LA-ICP-MS U–Pb dating results of quartz diorite and quartz monzodiorite, as well as Re–Os pyrite dating results of the Xinqiao Cu–S–Fe deposit to better understand the formation of these ore-forming intrusive rocks and their relationship to different metal deposits.

Regional geological setting

The Tongling region is situated along the northern margin of the Yangtze craton in central eastern China (Figure 1). Cambrian to Middle Triassic sedimentation developed on stable Precambrian basement, forming a thick sedimentary sequence that became country rocks for later Cu, Au, and Fe skarn deposits (Chang *et al.* 1991; Tang *et al.* 1998). The Indosinian-Yanshanian movements produced NE trending folds, faults and compressions. During the Yanshanian period (Jurassic/Cretaceous), this region became active again, which has long been interpreted as an intraplate deformational stage with abundant magmatisms. Intensive intermediate felsic rocks and associated hydrothermal activity formed multiple metal mineralizations (Chang *et al.* 1991; Tang *et al.* 1998).

Extensive marine depositions in the Tongling region, including clastic sedimentary rocks, carbonates, and evaporates, occurred from the Silurian through to Middle Triassic Periods (with the exception of Middle-Late Devonian). Mesozoic sedimentary-volcanic basins are widely distributed on these marine depositions (Chang *et al.* 1991; Tang *et al.* 1998) (Figure 1; Table 1). The strata, which are closely

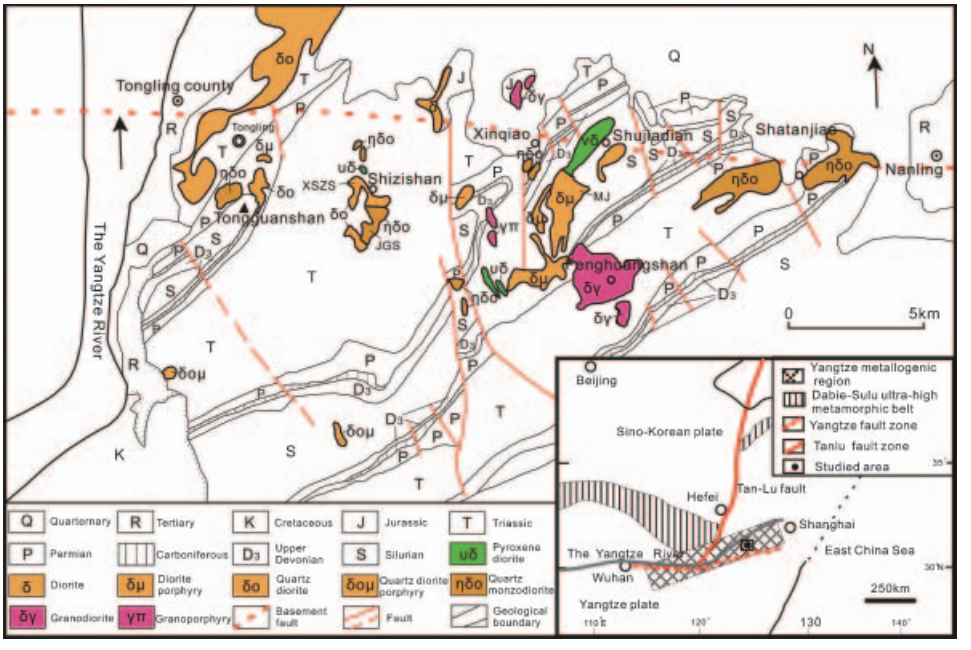

Figure 1. Geological sketch map of the Tongling metallogenic district, East China.

related to the metal deposits, are Carboniferous carbonate, Permian limestone and black shale, and Triassic carbonate and argillaceous rock (Anom 1987) (Table 1).

The Yanshanian magmatic rocks (J–K) are abundant in the region, forming more than 70 intrusions. These intrusions are mostly located within the Yangtze magmatic metallogenic belt controlled by the EW trending Tongling-Nanling deep fault (Figure 1) (Chang *et al.* 1991; Wu *et al.* 2003). There are three major rock associations:

Table 1. Strata cropping out in the Tongling area.

System	Series	Main lithology
Jurassic-Quaternary		Terrigenous clastic sedimentary rock
Triassic	Middle	Limestone, siltstone and dolomitic limestone
	Late	Primary limestone
Permian	Early	Top: primary siliceous rock and shale; bottom: primary quartz sandstone and fine sandstone
	Middle	Top: primary quartz sandstone, shale, dolomite and siliceous rock; bottom: primary biological detritus limestone
	Late	Top: thick-layer limestone; bottom: biological detritus-bearing limestone
Carboniferous	Early	Top: biological detritus limestone; bottom: huge thick-layer limestone
Devonian	Early	Primary quartz sandstone and siltstone
Silurian	Early	Primary fine sandstone
	Middle	Primary argillaceous rock, siltstone and fine sandstone
	Late	Primary shale and siltstone

Note: Source material derived from the Geological Map of the Tongling area, Anhui Province (1:50000).

(1) pyroxene diorite-pyroxene monzodiorite associations, related to Au mineralization; (2) quartz diorite-quartz monzodiorite associations, which are the most important magmatic rocks in the Tongling region primarily related to Cu–Au–Fe deposits; and (3) granodiorite associations, which are closely related to Cu-polymetallic deposits.

Samples

Three Yanshanian intermediate intrusions – Jiguanshi, Xishizishan and Miaojia – were sampled for this study. These intermediate intrusions are the most important magmatic rocks closely related to regional Cu–Au mineralization in the Tongling region (see Figure 1). Six pyrite ores were sampled from the Xinqiao Cu–S–Fe deposit in Tongling region for Re–Os dating.

Jiguanshi quartz monzodiorite

The Jiguanshi (JGS) quartz monzodiorite outcrop has an area of about 0.8 km^2, distributed along the border of Shizishan (E117°54′06.9″, N30°54′28.8″) (Figure 1). It intruded the Triassic limestone and dolomite. This quartz monzodioritic intrusion is grey in colour and is strongly altered. Silication, pyritization, chloritization, epidotization, argillization and carbonatization can be observed in thin sections. It has porphyritic texture. The modal mineralogy is mainly 40% plagioclase, 35% alkali-feldspar, 10% green hornblende, and 8–15% quartz, with a few traces of metal minerals, apatite, zircon and titanite (Figure 2(a) and (b)). Plagioclase is semi-euhedral to euhedral, with multiple twins, zoned texture, sodium-edge and fragmentation phenomena. Alkali-feldspar is anhedral, with Carsbad twin, poikilitic texture, zoned texture and sodium-edge. Hornblende surrounds alkali-feldspar, biotite, apatite, and metal minerals, probably the result of magma mixing. Most of the studied zircons from the Jiguanshi quartz monzodiorite (JGS) exhibit similar morphology, euhedral and about 100 μm in length with 1:1 to 3:1 in length/width ratio. Most crystals are prismatic, brown to slightly brown, and transparent to semi-transparent. The internal structure revealed by the CL images shows strong oscillatory zoning with small cores, similar to that of typical magmatic zircon (Figure 3(a)).

Xishizishan quartz diorite

The Xishizishan (XSZS) quartz diorite intrusion is located in south Shizishan (E117°52′53.1″, N30°54′50.8″) (Figure 1). This intrusion has an area of about 0.8 km^2. It intruded the Triassic limestone and dolomite. This intrusive rock is grey in colour, displays different grained texture, and consists of plagioclase (66–71%), K-feldspar (3–6%), quartz (1–7%), hornblende (10–17%), and biobite (1–3%), with a few traces of metal minerals, apatite, zircon and titanite (Figure 2(c) and (d)). Part of the intrusion is strongly altered, with silication, pyritization, chloritization, epidotization, argillization and carbonatization. All zircons from sample XSZS are euhedral and about 100 μm in length with 1:1 to 2:1 in length/width ratio. Most crystals are brown to slightly brown and transparent to semitransparent. The internal structure is similar to that of typical magmatic zircon (Figure 3(b)).

Miaojia diorite porphyry

Miaojia (MJ) diorite porphyry is located to the south of Shujiadian (E118°04′46.7″, N30°57′41.6″) (Figure 1). This intrusion has an area of about 2 km^2. It intruded into

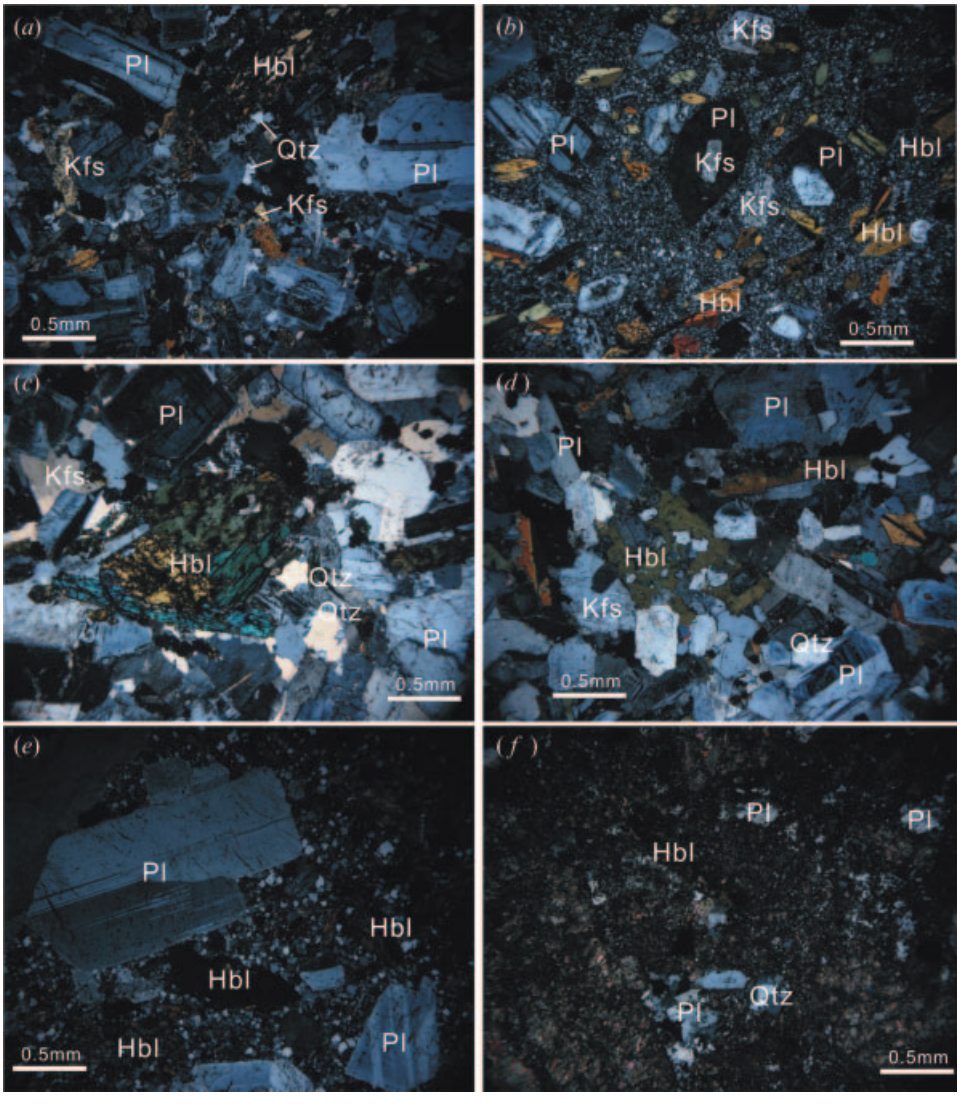

Figure 2. Photomicrographs illustrating minerals of the intermediate intrusive rocks in Tongling region. All the images were taken with the Leica microscope under polarized light conditions. The scale bar for each image is 0.50 mm. (a,b) plagioclase, alkali-feldspar, hornblende and quartz are the major mineral components of Jiguanshi quartz monzodiorite note the zoning texture of plagioclase and packing texture (plagioclase packing alkali-feldspar and hornblende); (c,d) plagioclase, potassic feldspar, hornblende and quartz are the major mineral components of Xishizishan quartz diorite, note the hornblende packing alkali-feldspar and plagioclase; (e,f) porphyritic texture of Miaojia diorite porphyry, phenocryst mainly consists of plagioclase, quartz, hornblende.
Note: Pl – plagiocalse; Kfs – potassic feldspar; Hbl – hornblende.

the Silurian sandstone and siltstone. This intrusive rock is grey in colour with porphyritic texture. Phenocryst mainly consists of plagioclase (10–25%), hornblende (8–15%) and quartz (5%). The matrix is cryptocrystalline-vitreous (Figure 2(e) and (f)). It is strongly altered, with all the feldspar altered through carbonatization and kaolinization. Zircons from Miaojia samples are similar to those in the Jiguanshi

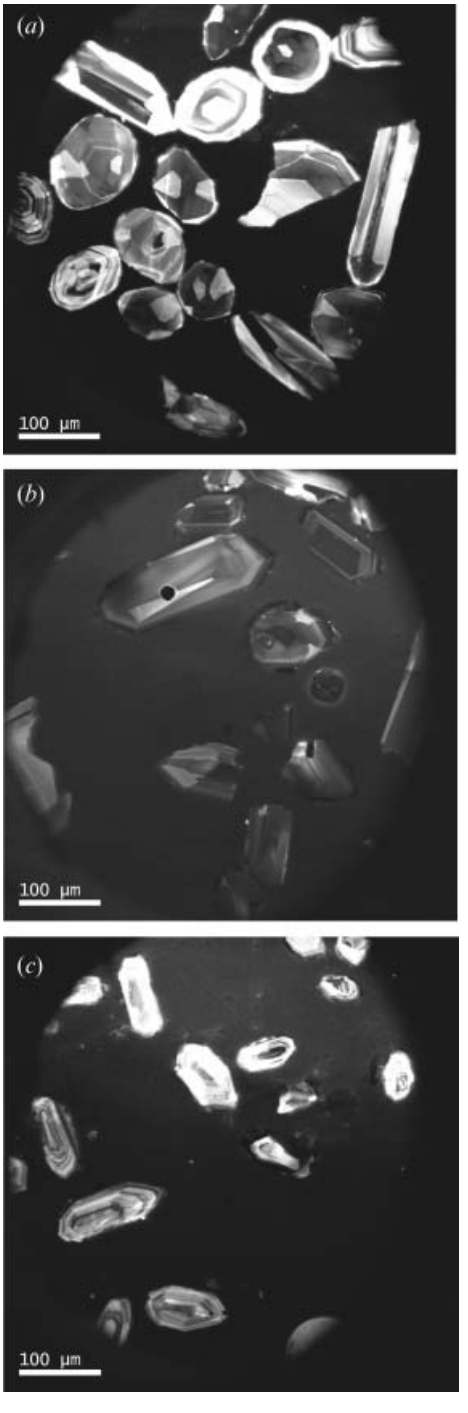

Figure 3. Cathodoluminescence (CL) images of representative zircons: (a) samples of Jiguanshi quartz diorite; (b) samples of Xishizishan quartz diorite; (c) samples of Miaojia diorite porphyry.

intrusion. They are euhedral and about 100 μm in length with 1:1 to 2:1 in length/width ratio. Most crystals are brown, transparent to semi-transparent, exhibiting the typical internal structure of magmatic CL images (Figure 3(c)).

Xinqiao deposit

The Cu–S–Fe–Au deposit at Xinqiao (XQ) is situated 24 km east of Tongling, Anhui Province, China (E117°59′32.5″, N30°55′23.5″) (Figure 1). It is a large-scale polymetallic deposit. The drilling exploration indicated a reserve of 0.5 million tonnes of Cu averaging 0.71%, 75.5 million tonnes of S averaging 29.3% and 24.9 million tonnes of Fe averaging 46%, and 11.2 tonnes of Au averaging at 4.7 g/tonne.

Sedimentary rocks cropping out in the Xinqiao deposit are of the Middle-Upper Silurian to Upper Permian in age (Figure 4). In most cases, the Upper Carboniferous is observed as the footwall of the sulphide orebody, and Qixia limestone is the hanging wall of stratiform mineralization. The Xinqiao deposit is located at the intersection of the northern limb of the Shujiadian anticline and the plunging part of the Dachengshan (or Niushan) anticline and the Shengchong syncline (Figures 1 and 4). There are two different types of sulphide mineralization at Xinqiao. One is the stratiform orebody restricted to a stratigraphic horizon, and the other is the skarn-type mineralization restricted to the contact of the Jitou stock

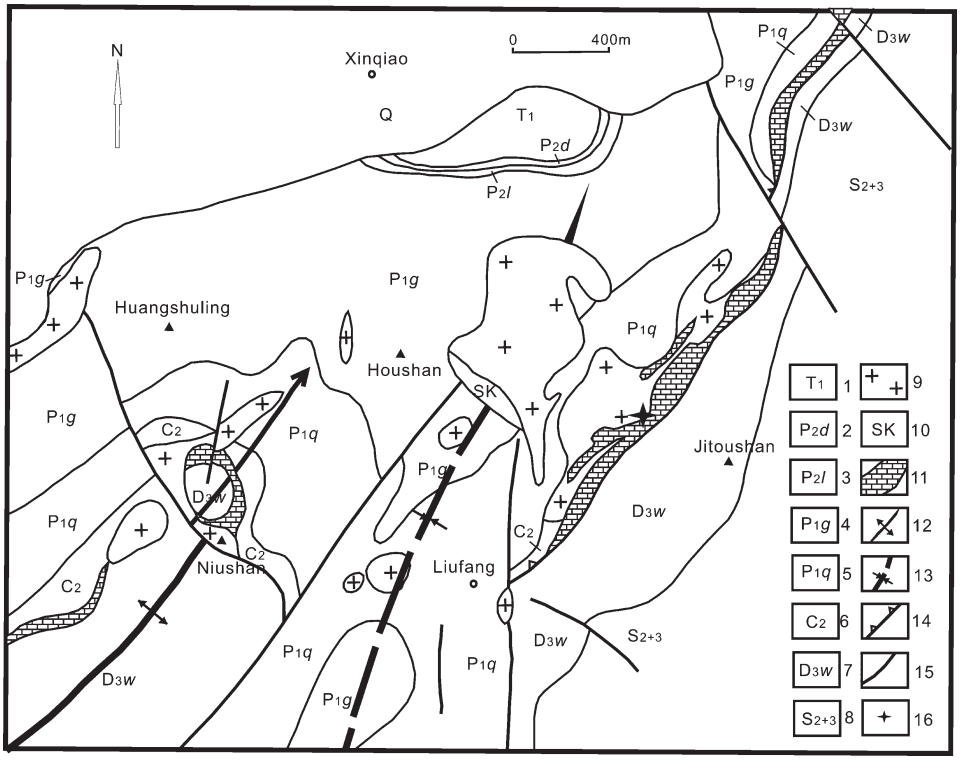

Figure 4. Geological map of Xinqiao orefield. 1: Lower Triassic; 2–5: Permian Dalong formation, Longtan formation, Gufeng formation and Qixia formation; 6: Upper Carboniferous; 7: Upper Devonian Wutong formation; 8: Middle–Upper Silurian; 9: intrusion; 10: skarn; 11: ore body; 12: Dachengshan anticline; 13: Shengchong syncline; 14: slipping structure; 15: fault; 16: sampling location.

with limestone host rock (see Figure 4). The ore in the Xinqiao deposit is dominated by massive pyrite with minor amounts of chalcopyrite, magnetite, pyrrhotite, galena, sphalerite, quartz and dolomite. Ore textures are primarily massive, consisting of more than 90% pyrite.

Analytical methods

LA-ICP-MS zircon analytical methods

Hand-picked zircon grains were mounted in epoxy, polished to half section to expose internal structures, and then cleaned for laser ablation inductively coupled plasma mass spectrometry (LA-ICP-MS) analysis. Zircon U–Th–Pb measurements using LA-ICP-MS were carried out at the State Key Laboratory of Continental Dynamics, Northwest University, Xi'an, China. The LA-ICP-MS for zircon *in situ* U–Pb dating consists of an ICP-MS (Elan 6100DRC) and an excimer laser ablation system (193 nm, GeoLas 200M, Lambda Physics). This combination has lower elemental fractionation than other kinds of laser ablation systems, such as 266 and 213 nm Nd: YAG laser system (Gao *et al.* 2002; Guillong *et al.* 2003), which is important for zircon U–Pb dating. The spot sizes applied were 30–40 μm in diameter.

Harvard standard zircon 91500 was used as an external standard for age calculation, NIST SRM 610 for concentrations and ^{29}Si for an internal standard. Because high purity argon (>99.995%) and helium (>99.995%) were used, both ^{204}Pb and ^{202}Hg intensities of blanks are always lower than 10 cps after 2 h gal line flushing (Yuan *et al.* 2004). Thus, interference of ^{204}Hg on ^{204}Pb is negligible. ^{204}Pb signals of zircons are generally not statistically significant. Detailed instrumentation and analytic accuracy descriptions are similar to those in the literature (Xing and Xu 1999; Gao *et al.* 2002; Yuan *et al.* 2003, 2004; Wang *et al.* 2006). The time-resolved spectra were processed off-line using Glitter software (ver 4.0, Macquarie University) to calculate the isotopic ratios. Common Pb was corrected by ComPbCorr#3_351 (Andersen 2002) for those with common ^{206}Pb>1%. The reported ages (Table 2; Figure 5) were calculated and Concordia diagrams were made using Isoplot/Ex_ver3.0 (Ludwig 2003).

Re–Os dating methods

Re–Os isotope analyses were carried out in the Re–Os Laboratory, National Research Centre of Geoanalysis, Chinese Academy of Geological Sciences. Detailed chemical separation procedures in this lab have been described in earlier literature (Du *et al.* 1994), but is briefly summarized here.

Enriched ^{190}Os and enriched ^{185}Re were obtained from the Oak Ridge National Laboratory. A weighed sample was loaded into a Carius tube through a thin neck long funnel. The mixed ^{190}Os and ^{185}Re spike solutions and 5 ml of 10M HCl, 15 ml of 16M HNO_3 and 30 ml of 30% H_2O_2 were loaded while the bottom part of the tube was frozen at -80 to -50°C in an ethanol-liquid nitrogen mixture, and the top was sealed using an oxygen-propane torch. The tube was then placed in a stainless-steel jacket and heated for 8 h at 230°C, and then for 16 h at 200°C After cooling, the bottom part of the tube was kept frozen, the neck of the tube was broken, the contents of the tube were poured into a distillation flask, and the residue was washed out with 40 ml water.

Table 2. LA-ICP-MS zircon analytical data for the intermediate intrusive rocks from the Tongling area.

Measured No.	Th	U	Th/U	$^{207}Pb/^{206}Pb$	1σ	$^{207}Pb/^{235}U$	1σ	$^{206}Pb/^{238}U$	1σ		$^{207}Pb/^{206}Pb$	$^{207}Pb/^{235}U$		$^{206}Pb/^{238}U$	
											1σ	(Ma)	1σ	(Ma)	1σ
JGS-01	177.14	254.42	1.436265101	0.04883	0.0022	0.14663	0.00639	0.02178	0.00025	140	79	139	6	139	2
JGS-02	86.68	127.44	1.470235348	0.04904	0.00315	0.15105	0.00946	0.02234	0.00033	150	114	143	8	142	2
JGS-03	263.18	263.47	1.001101907	0.04875	0.00203	0.15115	0.00607	0.02249	0.00025	136	73	143	5	143	2
JGS-04	255.42	250.24	0.979719677	0.0537	0.00206	0.15744	0.00577	0.02127	0.00023	358	63	148	5	136	1
JGS-05	167.88	225.2	1.341434358	0.04871	0.00225	0.14667	0.00654	0.02185	0.00025	134	81	139	6	139	2
JGS-06	230.33	243.97	1.059219381	0.04868	0.00295	0.13868	0.00815	0.02068	0.0003	132	105	132	7	132	2
JGS-07	306.49	305.61	0.997128781	0.0486	0.00211	0.13671	0.00573	0.02042	0.00023	129	76	130	5	130	1
JGS-08	162.58	208.63	1.283245172	0.04872	0.00222	0.14545	0.00639	0.02167	0.00025	134	80	138	6	138	2
JGS-09	189.3	209.43	1.106339144	0.0488	0.0032	0.14317	0.00912	0.02129	0.00033	138	114	136	8	136	2
JGS-10	221.96	254.25	1.145476662	0.04874	0.00254	0.14839	0.00749	0.0221	0.00028	135	91	140	7	141	2
JGS-11	60.83	94.05	1.546112116	0.04919	0.00569	0.16573	0.01871	0.02445	0.00064	157	204	156	16	156	4
JGS-12	605.92	397.53	0.65607671	0.04861	0.00239	0.13634	0.00649	0.02036	0.00026	129	85	130	6	130	2
JGS-13	174.44	192.89	1.105767026	0.04898	0.0036	0.15178	0.01083	0.02249	0.0004	147	127	143	10	143	3
JGS-14	234.5	228.66	0.975095949	0.04855	0.00441	0.13293	0.01176	0.01987	0.00043	126	157	127	11	127	3
JGS-15	236.62	399.37	1.687811681	0.05997	0.0011	0.99259	0.01664	0.12009	0.00093	602	23	700	8	731	5
JGS-16	88.81	137.47	1.547911271	0.04896	0.00344	0.14882	0.01017	0.02205	0.00038	146	122	141	9	141	2
JGS-17	159.99	192.42	1.202700169	0.04682	0.00276	0.14492	0.00832	0.02245	0.00032	40	98	137	7	143	2
JGS-18	412.38	338.87	0.821742083	0.0475	0.00343	0.13803	0.00968	0.02108	0.00037	74	122	131	9	134	2
XSZS-01	542.87	306.11	0.563873487	0.04872	0.00249	0.14072	0.00695	0.02096	0.00027	134	89	134	6	134	2
XSZS-02	616.82	329.97	0.534953471	0.04756	0.00237	0.14107	0.0068	0.02152	0.00026	77	84	134	6	137	2
XSZS-03	359.07	212.77	0.592558554	0.04857	0.00394	0.12973	0.01025	0.01937	0.00036	127	142	124	9	124	2
XSZS-04	378.11	282.65	0.747533786	0.04853	0.0035	0.13314	0.00934	0.0199	0.00034	125	125	127	8	127	2
XSZS-05	1160.67	502.15	0.432638045	0.04834	0.00283	0.12899	0.00732	0.01935	0.00028	116	100	123	7	124	2
XSZS-06	446.44	331.6	0.742764985	0.0483	0.00382	0.11881	0.00916	0.01783	0.00033	114	137	114	8	114	2
XSZS-07	313.58	224.53	0.71602143	0.04858	0.00303	0.13327	0.00809	0.01989	0.0003	128	108	127	7	127	2
XSZS-08	226.02	191.5	0.847270153	0.06183	0.01192	0.17078	0.03261	0.02003	0.00053	668	415	160	28	128	3
XSZS-09	333.58	236.51	0.709005336	0.04855	0.00272	0.1398	0.0076	0.02087	0.00029	126	97	133	7	133	2
XSZS-10	556.02	367.05	0.660138125	0.06175	0.00561	0.19718	0.01765	0.02316	0.00036	665	202	183	15	148	2
XSZS-11	887.8	475.89	0.53603289	0.04865	0.00187	0.14222	0.00525	0.02118	0.00023	131	66	135	5	135	1

Table 2. (*Continued.*)

Measured No.	Th	U	Th/U	$^{207}Pb/^{206}Pb$		$^{207}Pb/^{235}U$		$^{206}Pb/^{238}U$		$^{207}Pb/^{206}Pb$	$^{207}Pb/^{235}U$		$^{206}Pb/^{238}U$	
					1σ		1σ		1σ		1σ	(Ma)	1σ	(Ma)	1σ
XSZS-12	637.44	365.16	0.572853916	0.0463	0.00207	0.13681	0.00592	0.02141	0.00025	13	69	130	5	137	2
XSZS-13	419.62	258.29	0.615533101	0.04635	0.00289	0.13005	0.00789	0.02032	0.0003	16	103	124	7	130	2
XSZS-14	744.47	397.44	0.5338563	0.04378	0.00182	0.13347	0.00536	0.02208	0.00024	-82	66	127	5	141	2
XSZS-15	771.34	531.01	0.688425338	0.04628	0.00162	0.13996	0.00472	0.02191	0.00022	12	52	133	4	140	1
XSZS-16	455.47	297.9	0.654049663	0.04627	0.00229	0.13226	0.00634	0.02071	0.00026	12	78	126	6	132	2
XSZS-17	534.38	446.58	0.835697444	0.05385	0.00301	0.15974	0.00862	0.02149	0.00032	365	95	150	8	137	2
XSZS-18	424.34	360.44	0.849413206	0.04674	0.00203	0.14946	0.00628	0.02317	0.00027	36	68	141	6	148	2
XSZS-19	431.62	292.38	0.677401418	0.04652	0.00207	0.14268	0.00615	0.02222	0.00026	25	70	135	5	142	2
XSZS-20	705.06	379.1	0.537684736	0.04195	0.00201	0.12971	0.00604	0.0224	0.00027	-180	84	124	5	143	2
MJ-01	152.5	176.22	1.155540984	0.04907	0.0035	0.15364	0.01066	0.02271	0.00037	151	126	145	9	145	2
MJ-02	151.68	187.72	1.237605485	0.04869	0.00261	0.1392	0.00722	0.02073	0.00027	133	94	132	6	132	2
MJ-03	167.6	169.76	1.012887828	0.04868	0.00252	0.1412	0.00711	0.02103	0.00026	132	92	134	6	134	2
MJ-04	217.95	242.26	1.111539344	0.04866	0.00274	0.13807	0.00753	0.02058	0.00028	131	98	131	7	131	2
MJ-05	216.1	207.58	0.960573808	0.05791	0.00353	0.17017	0.01004	0.02131	0.00033	526	102	160	9	136	2
MJ-06	150.92	160.59	1.064073681	0.05279	0.00277	0.15309	0.00778	0.02103	0.00027	320	92	145	7	134	2
MJ-07	83.87	116.94	1.394300703	0.04922	0.00334	0.15493	0.01028	0.02283	0.00033	158	123	146	9	146	2
MJ-08	200.34	185.5	0.925925926	0.06812	0.00184	1.13106	0.02872	0.1204	0.00116	872	37	768	14	733	7
MJ-09	164.83	180.7	1.096281017	0.04877	0.00267	0.14225	0.00758	0.02115	0.00027	137	98	135	7	135	2
MJ-10	111.04	167.14	1.505223343	0.04611	0.00254	0.13445	0.00725	0.02115	0.00024	4	120	128	6	135	2
MJ-11	207.72	187.59	0.903090699	0.04901	0.00418	0.16069	0.01337	0.02378	0.00046	148	151	151	12	152	3
MJ-12	200.72	198.09	0.98689717	0.04878	0.00232	0.1472	0.00676	0.02188	0.00026	137	83	139	6	140	2
MJ-13	78.01	84.78	1.086783746	0.04877	0.00368	0.14363	0.01058	0.02136	0.00036	137	134	136	9	136	2
MJ-14	141.75	149.11	1.051922399	0.04922	0.00312	0.15008	0.00926	0.02211	0.00032	158	113	142	8	141	2
MJ-15	180.35	189.22	1.049182146	0.05046	0.00275	0.14101	0.00746	0.02027	0.00027	216	98	134	7	129	2
MJ-16	106.63	157.64	1.478383194	0.04912	0.0033	0.14128	0.00924	0.02086	0.00033	154	118	134	8	133	2
MJ-17	163.75	201.05	1.22778626	0.04884	0.0028	0.14579	0.00812	0.02165	0.0003	140	101	138	7	138	2
MJ-18	185.22	213.83	1.154464961	0.04903	0.0035	0.15155	0.01051	0.02242	0.00038	149	125	143	9	143	2
MJ-19	267.91	226.45	0.845246538	0.04868	0.00307	0.14649	0.00899	0.02182	0.00032	132	111	139	8	139	2
MJ-20	109.18	170.95	1.56576296	0.05031	0.00309	0.21164	0.01263	0.03051	0.00046	209	109	195	11	194	3

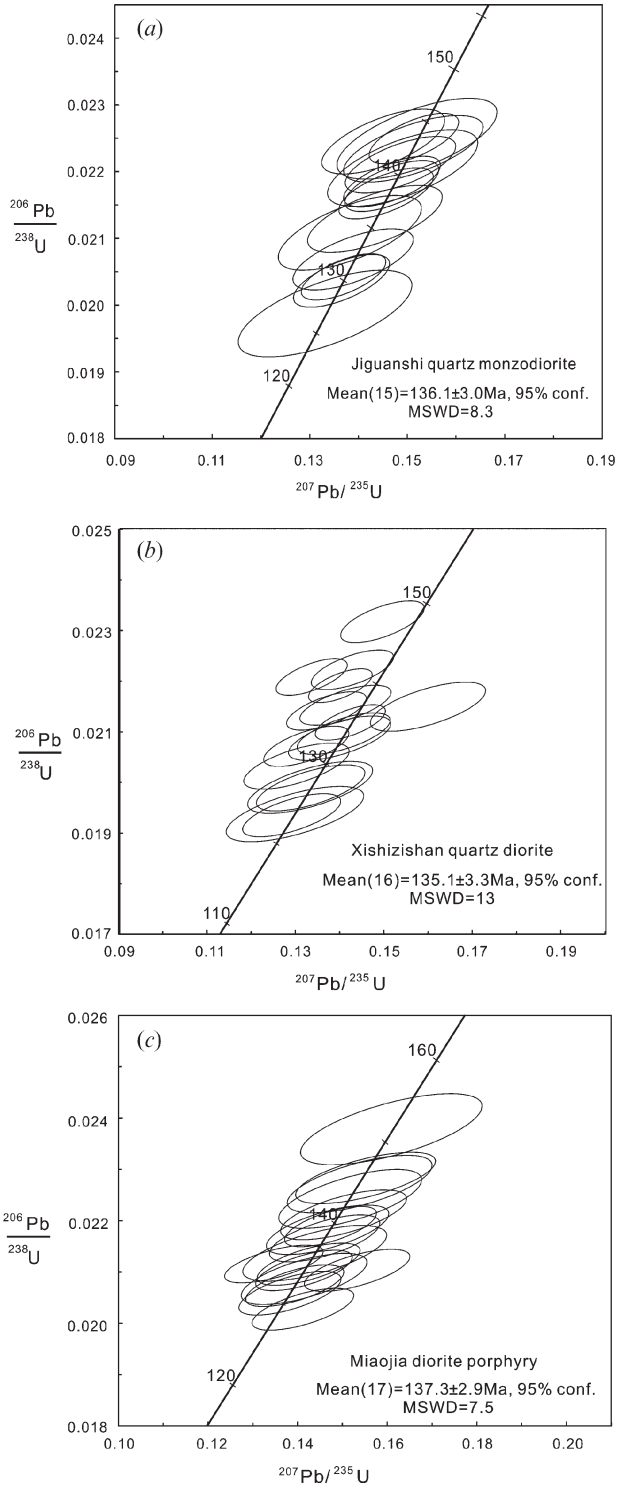

Figure 5. U–Pb concordia diagrams for the intermediate intrusions: (a) Jiguanshi quartz monzodiorite; (b) Xishizishan quartz diorite; (c) Miaojia diorite porphyry.

Osmium was distilled twice for purification. In the first distillation step, OsO_4 was distilled at 105 to 110°C for 50 min and trapped in 10 ml water. The residual Re-bearing solution was saved in a 150 ml beaker for Re separation. The water trap solution plus 40 ml water were distilled again. The OsO_4 was distilled for 1 h and trapped in 10 ml water for ICP-MS (TJA PQ ExCell) determination of Os isotope ratios.

The Re-bearing solution was evaporated to near dryness, and 1 ml water was added twice with heating to near dryness in between. Ten millilitres of 5M NaOH was added to the residue followed by Re extraction with 50 ml acetone in a 120 ml Teflon separation funnel. The water phase was then discarded and the acetone phase washed with 2 ml of 5M NaOH. The acetone phase was transferred to a 100 ml beaker that contained 2 ml water. After evaporation to dryness, the Re was picked up in 1 ml water for the ICPMS determination. Cation-exchange resin was used to remove Na if the salinity of the Re-bearing solution was more than 1 mg/ml (Du *et al.* 1994).

Average blanks for the total Carius tube procedure described above were ca. 50 pg for Re and ca. 5 pg for Os. The uncertainty in each individual age determination was about 1.4%, including the uncertainty of the decay constant of ^{187}Re, uncertainty in isotope ratio measurement, and spike calibrations (Du *et al.* 1994). The decay constant was $\lambda\,(^{187}Re) = 1.666 \times 10^{-11}$/year (Smoliar *et al.* 1996). The final uncertainties of ages are 2σ absolute, including errors on Re and ^{187}Os concentrations and the uncertainty in the ^{187}Re decay constant. The results are listed in Table 3.

Major and trace elements analytical methods

Major elements of whole rock samples were analysed by XRF and trace elements including rare earth elements were analysed by ICP-MS in the Physics and Chemistry Laboratory Centre of the University of Science and Technology of China. The relative deviations of the results relative to the reference values for standards used in our study are typically below 10%. LA-ICP-MS method was applied to analyse trace elements of zircon, and the uncertainty is less than 10% (Yuan *et al.* 2004). The results are listed in Tables 4 and 5.

Analytical results

LA-ICP-MS analytical results

All 18 zircon analyses for sample JGS have Th/U ratios of 0.66–1.69, with Th concentrations of 86.7–606 ppm, U concentrations of 94.1–399 ppm, showing characteristics of typical magmatic zircons. Spot JGS-15 has Th concentration of 237 ppm, U concentration of 399 ppm, with Th/U ratios of 1.69. This zircon grain has a core with heterogeneously spotted and esturary texture and an edge with weak oscillatory zoning. It is an inherited zircon from Neoproterozoic protoliths with $^{206}Pb/^{238}U$ apparent age of 731 ± 5 Ma, which is common in the northern margin of the South China Block (Li *et al.* 2003; Sun *et al.* 2003; Zhou *et al.* 2006). The $^{206}Pb/^{238}U$ age for 15 spots range from 127 ± 3 to 143 ± 2Ma. These 15 spots are concordant, with a mean $^{206}Pb/^{238}U$ age of 136.1 ± 3.0 Ma (95% confidence, MSWD = 8.3; Figure 5(a)). Their $^{206}Pb/^{238}U$ ages can be divided into an older group (mean 139.1 ± 1.9 Ma) and younger group (mean 132.2 ± 1.6 Ma), likely representing two crystallization periods. Analyses of spots JGS-04 and JGS-11 show lead loss.

Table 3. Re–Os date of pyrite from Xinqiao Cu–S–Fe ore deposit in Tongling region by ICP-MS analysis.

		Re (ng/g)		Common Os (ng/g)		^{187}Os (ng/g)		^{187}Re/^{188}Os		^{187}Os/^{188}Os	
Sample	Weight (g)	Measured	2σ	Measured	2σ	Measured	2σ	Measured	2σ	Measured	2σ
xq01	1.202	6.057	0.052	0.0024	0.0001	0.0082	0.0001	12231	606	26.2	1.3
xq02	1.201	18.74	0.35	0.0084	0.0001	0.0260	0.0002	10692	244	23.58	0.26
xq03	1.209	86.34	4.933	0.0138	0.0002	0.1183	0.0009	29860	1784	65.11	1.04
xq04	1.199	85.24	1.00	0.0616	0.0006	0.1272	0.0010	6615	103	15.71	0.12
xq05	1.199	10.57	0.13	0.0038	0.0001	0.0145	0.0001	13314	247	28.99	0.39
Xq06	1.200	2.746	0.031	0.0024	0.0001	0.0037	0.0003	5535	258	12.00	1.04

Note: Decay constant: λ (^{187}Re) $=1.666\times10^{-11}$/year (Smoliar *et al.* 1996).

Table 4. Compositions of intermediate intrusive rocks from the Tongling area, Anhui Province.

	Wls	Hc	Jgs	Jkl	Tebd	Jc	Hs	Bc	Xszs	Mj	Stj	Xqt	Tgs
Major oxides (wt-%)													
SiO_2	62.11	64.08	59.07	63.41	61.07	53.62	61.54	59.46	57.29	54.13	59.83	60.87	63.02
TiO_2	0.65	0.59	0.86	0.57	0.74	0.54	0.71	0.78	0.95	0.87	0.71	0.57	0.54
Al_2O_3	16.26	15.43	16.67	16.61	16.28	17.11	16.14	16.05	16.66	15.45	16.80	16.99	16.32
Fe_2O_3	5.21	3.28	6.47	4.72	5.13	4.30	5.79	5.42	6.15	6.07	5.28	6.49	4.56
MnO	0.09	0.05	0.16	0.09	0.10	0.10	0.11	0.07	0.08	0.22	0.09	0.06	0.08
MgO	1.75	1.49	2.26	1.43	2.09	1.54	2.14	2.08	2.51	2.55	2.04	1.84	1.50
CaO	4.88	4.99	5.93	4.66	5.65	5.66	4.57	4.89	5.83	6.61	5.31	1.88	4.42
Na_2O	4.27	4.27	3.92	4.53	4.05	1.38	4.17	3.80	3.67	0.70	4.78	4.83	4.60
K_2O	2.74	3.42	2.77	2.44	3.21	4.27	2.66	3.39	3.03	4.71	2.28	3.65	2.55
P_2O_5	0.27	0.23	0.35	0.25	0.29	0.30	0.35	0.31	0.41	0.37	0.32	0.20	0.24
Total	98.23	97.83	98.46	98.71	98.61	88.82	98.18	96.25	96.58	91.68	97.44	97.38	97.83
Trace elements (ppm)													
La	31.2	16.7	37.9	28.8	38.5	73.1	43.7	31.6	35.8	38	27.2	11.7	27
Ce	60.1	37.3	70.8	58	74.4	132	84.1	70.3	76.9	77	54.6	21.5	45.3
Pr	7.22	4.05	8.22	6.84	8.69	14.5	10.1	8.53	9.27	9.01	7.94	3.52	5.83
Nd	28.5	16.4	32.9	27.7	34.6	54.2	40.1	33.8	37.9	35.4	32.8	15.4	24.7
Sm	4.96	2.85	5.62	4.69	6.04	8.38	6.6	5.77	6.48	5.8	5.71	2.89	4.05
Eu	1.62	1.1	1.78	1.56	1.78	2.52	1.95	1.66	2.06	1.71	1.67	1.45	1.43
Gd	4.21	2.58	4.99	3.79	5.18	7.19	5.71	4.97	5.71	5	4.73	2.59	3.34
Tb	0.576	0.355	0.712	0.516	0.736	0.995	0.807	0.725	0.835	0.686	0.67	0.334	0.427
Dy	3.09	2.02	3.95	2.59	4	5.09	4.38	3.92	4.36	3.61	3.52	1.71	2.27
Ho	0.567	0.387	0.755	0.448	0.74	0.932	0.81	0.724	0.795	0.671	0.64	0.28	0.378
Er	1.65	1.2	2.18	1.29	2.25	2.72	2.36	2.13	2.26	1.99	1.83	0.763	1.054
Tm	0.265	0.199	0.363	0.191	0.354	0.463	0.396	0.363	0.365	0.336	0.287	0.112	0.166
Yb	1.71	1.43	2.36	1.3	2.3	2.95	2.44	2.26	2.23	2.14	1.8	0.694	1.07
Lu	0.242	0.198	0.331	0.176	0.323	0.441	0.337	0.332	0.298	0.298	0.238	0.08	0.138
REE	145.91	86.77	172.86	137.89	179.89	305.48	203.79	167.08	185.26	181.65	143.64	63.02	117.15
δEu	1.08	1.24	1.03	1.13	0.97	0.99	0.97	0.95	1.04	0.97	0.98	1.62	1.19
La/Yb_N	12.30	7.87	10.83	14.94	11.29	16.71	12.07	9.43	10.82	11.97	10.19	11.37	17.01
Sc	12.3	23.3	12.1	7.6	11.3	4.77	10.4	12.5	14.6	13.6	12.4	8.22	7.7

Table 4. (*Continued.*)

	Wls	Hc	Jgs	Jkl	Tebd	Jc	Hs	Bc	Xszs	Mj	Stj	Xqt	Tgs
V	76.2	86.7	107	48.7	69.7	59.7	73.3	101	108	94.4	74.6	67.5	46.7
Cr	3.01	3.22	0.619	2.81	6.53	−0.522	1.32	4.38	1.89	3.9	6.71	21	3.76
Co	90.5	135	83.6	76.3	93.9	28.7	91.3	82.4	54	40.8	78.4	65.4	88.2
Ni	4.46	7.16	3.87	4.3	9.19	1.82	4.2	5.23	5.29	7.34	7.03	25.3	4.87
Cu	11.6	164	25.6	9.16	20	121	10.4	164	79.1	33.4	126	23.2	11.6
Zn	281.7	634.2	103.9	133.1	181.8	313	98.31	185	185.3	247.7	227.4	241.6	43.51
Rb	68.9	51.2	77.8	40.2	87.8	142	73.3	94.5	89.3	280	30.7	74.9	52.7
Sr	907	708	813	1092	884	339	876	801	878	264	959	483	958
Y	19.3	23.6	25.9	14.4	25.2	29.7	26.4	24	25.3	21.8	19.7	8.52	13.7
Zr	47.7	170	24.2	16	34.3	289	42.8	29.5	25.9	95.9	18	24.4	28.5
Nb	14.9	15.5	13.1	13.8	16.1	24.2	16.7	14.9	15.7	13.6	17.7	12.4	14.2
Mo	0.91	2.09	1.61	1.27	0.56	3.02	3.22	0.66	2.45	0.47	2.58	3.27	4.61
Ba	944.3	1277.3	640.1	952.4	990.6	827.5	923.1	800.3	743.2	935.3	741.5	1116	907.2
Hf	1.99	5.53	1.35	1.07	1.72	7.84	1.97	1.54	1.56	3.83	0.947	1.15	1.49
Ta	1.02	2.33	0.782	0.781	1.02	1.2	1.01	1.03	0.963	0.876	0.981	1.36	0.705
Pb	28.74	11.33	8.84	11.25	19.76	240	9.82	8.99	8.81	4.86	6.56	2.65	6.42
Th	7.22	8.01	9.3	6.19	8.5	17.6	8.08	9.35	9.24	10.2	5.11	2.84	6.01
U	1.79	2.32	2.15	1.56	1.58	4.56	1.93	2.1	1.96	1.96	1.95	0.712	1.63
Nb/Ta	14.61	6.65	16.75	17.67	15.78	20.17	16.53	14.47	16.30	15.53	18.04	9.12	20.14
Pb/Nd	1.01	0.69	0.27	0.41	0.57	4.43	0.24	0.27	0.23	0.14	0.20	0.17	0.26

Table 5. Rare earth elements and trace elements of zircons analysed by LA-ICP-MS.

Sample	P	Ti	Cr	Rb	Sr	Y	Nb	La	Ce	Pr	Nd	Sm	Eu	Gd	Tb	Dy	Ho	Er	Tm	Yb	Lu	Ta	δCe	$(La/Yb)_N$	δEu
JGS-01	128.11	9.62	<3.89	0.301	0.216	1101.83	3.26	<0.0185	35.71	0.099	1.73	2.9	1.73	15.84	6.25	80.07	34.12	171.31	39.55	414.17	89.28	0.728	96.54	3.01841E-05	0.78
JGS-02	155.65	6.52	<3.87	<0.27	0.12	630.22	1.04	<0.028	18.35	0.13	1.77	2.64	1.53	11.99	3.93	48.66	19.5	96.88	22.95	247.54	54.42	0.285	37.41	7.64361E-05	0.83
JGS-03	168.3	10.97	<3.89	0.32	0.159	1367.14	2.52	<0.028	41.11	0.257	3.7	6.08	3.33	28.54	9.73	112.95	43.54	204.33	44.76	457.88	94.02	0.595	44.01	4.1323E-05	0.77
JGS-04	141.86	14.32	<3.52	0.281	0.585	1295.68	2.18	0.06	35.54	0.271	4.42	6.68	3.7	28.51	9.37	108.64	41.45	193.61	42.45	439.21	89.92	0.537	34.68	9.23134E-05	0.82
JGS-05	146.25	10.26	<4.01	<0.26	0.204	957.64	2.29	<0.022	27.59	0.121	1.68	2.77	1.57	13.89	5.13	67.07	28.68	147.04	34.74	375.97	81.22	0.485	61.13	3.95417E-05	0.77
JGS-06	118.57	9.36	<3.11	0.23	0.179	1123.86	1.44	0.035	23.98	0.317	4.47	7.04	3.65	25.91	7.93	91.16	34.72	167.34	38.33	418.86	87.65	0.325	20.80	5.64657E-05	0.83
JGS-07	191.67	12.14	<3.33	0.337	0.207	1557.27	3.04	<0.021	49.65	0.168	2.75	5.13	3.3	30.56	10.71	127.44	49.79	231.76	51.03	522.33	105.1	0.714	80.84	2.71681E-05	0.81
JGS-08	160.95	8.96	<3.62	<0.240	0.153	1006.9	2.12	0.0224	29.31	0.13	2.22	3.86	2.17	18.21	6.44	78.5	31.68	155.33	35.72	377.13	79	0.521	60.65	4.01368E-05	0.79
JGS-09	154.57	10.76	<3.44	0.29	0.19	882.25	1.65	0.051	26.03	0.182	2.76	4.31	2.4	17.94	6.12	71.32	27.92	132.76	30.43	320.6	65.78	0.428	37.07	0.000107496	0.83
JGS-10	138.18	10.62	<4.24	<0.27	0.153	551.65	1.36	0.059	24.24	0.127	1.49	1.91	1.2	9.58	3.34	41.45	16.84	82.15	19.03	199.36	40.78	0.449	46.57	0.000199986	0.86
JGS-11	155.75	6.47	<4.28	<0.32	<0.108	502.8	0.88	<0.029	12	0.076	1.26	2.09	1.12	9.74	3.29	39.5	15.61	76.34	17.99	197.84	41.62	0.299	39.57	9.90534E-05	0.76
JGS-12	137.27	11.62	<3.13	<0.22	0.196	1220.62	2.73	0.033	52.79	0.242	3.39	4.81	2.85	22.77	7.68	90.98	36.71	181.51	42.29	452.78	95.09	0.513	59.43	4.92507E-05	0.83
JGS-13	145.64	9.11	<4.12	<0.28	0.21	761.6	1.66	0.138	27.01	0.12	1.23	2.21	1.29	12.17	4.38	52.97	22.71	114.94	27.42	299.89	65.22	0.367	45.09	0.000310959	0.76
JGS-14	164.51	21.08	<4.90	<0.33	0.45	882.33	1.72	0.371	29.08	0.45	4.19	4.9	3.46	17.92	6.3	72.61	27.55	129.2	28.89	296.33	61.7	0.434	14.15	0.000846026	1.13
JGS-15	915.31	5.02	<3.25	0.53	0.478	2694.09	8.69	6.95	42.93	2.58	15.51	10.01	0.66	50.01	18.97	239.27	95.03	420.27	83.32	764.56	139.28	2.3	2.38	0.006142694	0.09
JGS-16	197.88	7.59	<3.38	<0.26	0.114	667.18	1.07	0.029	17.76	0.074	1.27	2.7	1.51	11.46	4.21	50.23	20.58	103.79	24.51	272.16	58.68	0.327	59.95	7.20044E-05	0.83
JGS-17	138.33	8.68	<4.22	<0.29	0.154	708.03	1.15	0.034	19.01	0.148	2.04	3.14	1.89	13.46	4.33	52.51	20.96	105.56	25.26	275	60.9	0.265	33.87	8.35472E-05	0.89
JGS-18	167.44	12.19	<4.34	<0.33	0.42	1661.24	2.16	0.181	46.89	0.643	8.48	11.72	6.39	40.9	12.62	139.88	52.09	239.89	53.98	570.31	113.15	0.425	18.89	0.000214463	0.89
XSZS-01	297.59	8.57	<4.48	<0.33	0.183	1906.05	2.05	0.102	71.11	0.804	12.1	19.91	8.26	72.61	20.09	197.84	65.64	271.05	53.64	503.51	96.71	0.368	24.18	0.000136892	0.66
XSZS-02	328.47	7.96	<4.52	0.41	0.224	2138.46	2.15	0.142	85.37	0.992	16.3	24.74	10.2	84.59	23	226.07	73.83	304.25	60.05	557.91	106.47	0.44	23.39	0.000171993	0.68
XSZS-03	223.06	8.59	<5.03	<0.37	0.232	1435.08	1.35	0.087	54.67	0.775	11.17	16.97	6.6	56.93	15.17	148.36	49.58	208.61	41.23	387.73	76.32	0.29	19.38	0.000151627	0.65
XSZS-04	287.41	10.93	<5.01	<0.36	0.157	1323.13	2.95	<0.033	69.95	0.173	3.27	5.98	2.79	30.43	10.1	116.82	43.48	195.7	40.81	393.24	77.63	0.581	108.07	5.67077E-05	0.63
XSZS-05	321.55	11.64	<4.36	0.35	0.172	1160.65	2.81	<0.030	82.07	0.226	4.49	7.95	3.4	35.5	10.61	113.29	38.93	164.73	32.96	309.22	59.52	0.564	99.06	6.55601E-05	0.62
XSZS-06	272.84	8.31	<4.04	0.36	0.198	1830.93	1.78	0.116	62.57	0.834	11.99	18.98	7.82	67.39	18.78	188.35	61.83	259.63	52.19	493.89	95.32	0.367	20.42	0.000158713	0.67
XSZS-07	267.99	5.95	<4.17	<0.29	0.143	1325.58	1.47	0.048	51.66	0.493	7.65	12.11	5.04	45.37	12.95	131.71	44.93	190.86	38.28	374.84	71.35	0.344	28.95	8.65328E-05	0.66
XSZS-08	169.21	7.75	<4.16	0.53	0.77	948.46	1.07	0.314	36.86	0.388	6.65	9.6	4.07	34.85	9.73	95.78	33.12	138.89	28.36	268.3	51.92	0.206	20.89	0.000790851	0.68
XSZS-09	191.55	5.67	<2.87	0.22	0.156	1454.75	1.48	0.05	56	0.588	9.23	13.95	5.49	51.43	14.19	146.77	50.09	211.82	42.57	397.87	75.46	0.381	26.43	8.49209E-05	0.63
XSZS-10	283.05	11.91	<3.91	2.05	0.602	1565.52	3.06	0.282	73.95	0.545	7.37	12.63	5.53	50.95	14.54	151.33	52.6	224.55	45.58	437.09	85.29	0.532	32.56	0.000435977	0.67
XSZS-11	338.22	12.98	<3.70	0.43	0.231	1832.34	4.83	0.037	134.7	0.317	5.08	9.74	4.46	50.95	16.17	175.94	62.5	265.65	53.5	497.1	93.67	0.767	116.56	5.02972E-05	0.61
XSZS-12	820.98	8.55	<4.36	0.43	6.62	2149.32	2.78	1.91	98.05	1.029	13.95	21.68	8.93	79.1	22.04	221.14	73.86	306.54	60.95	567.83	107.69	0.511	16.12	0.002273006	0.66
XSZS-13	479.76	8.85	<3.86	1.8	1.96	1686.81	1.71	2.8	71.55	1.481	14.86	19.58	7.62	65.22	17.59	174.79	58.05	241.13	48.5	456.79	85.99	0.373	8.11	0.004142162	0.65
XSZS-14	356.31	8.15	<3.94	0.36	0.22	2537.6	2.61	0.125	101	1.081	18.12	27.82	11.9	100.8	27.55	268.5	88	358.89	70.45	659.63	124.6	0.472	25.64	0.000128055	0.69

Table 5. (*Continued.*)

Sample	P	Ti	Cr	Rb	Sr	Y	Nb	La	Ce	Pr	Nd	Sm	Eu	Gd	Tb	Dy	Ho	Er	Tm	Yb	Lu	Ta	δCe	$(La/Yb)_N$	δEu
XSZS-15	283.72	11.39	<3.82	0.35	0.284	2100.05	7.01	0.037	175.7	0.255	4.44	9.02	4.06	47.36	16.02	185.78	69.7	310.1	63.19	607.01	113.26	1.015	187.17	4.119E-05	0.60
XSZS-16	340.97	6.94	<3.86	<0.28	0.227	1630.35	2.26	0.044	61.98	0.392	6.22	11.79	5.56	52.96	15.67	161.8	55.55	239.11	48.27	461.4	87.86	0.465	43.45	6.44408E-05	0.68
XSZS-17	249.19	8.52	<4.29	<0.32	0.234	1665.33	5.83	<0.032	128.6	0.216	3.7	6.81	3.16	32.12	11.12	134.99	53.42	247.54	52.75	513.16	98.88	0.875	161.55	4.21389E-05	0.65
XSZS-18	205.34	4.82	<4.05	<0.30	0.164	929.26	3.46	<0.027	92.56	0.136	2.31	4.58	2.04	21.42	7.01	78.98	30.19	137.25	29.61	294.78	56.92	0.698	181.42	6.18944E-05	0.63
XSZS-19	267.94	11.39	<4.17	<0.29	0.251	1566.83	2.72	0.047	72.17	0.418	6.43	10.65	4.56	45.13	13.44	145.17	52.02	228.76	46.88	450.09	87.7	0.495	47.44	7.05641E-05	0.64
XSZS-20	264.58	9.43	<3.61	<0.26	0.246	1733.56	2.53	0.065	84.93	0.565	8.81	15.16	6.56	62.21	17.66	176.27	60.03	251.24	50.47	469.95	88.54	0.572	41.27	9.34646E-05	0.65
MJ-01	137.73	7.14	<4.46	<0.28	0.181	583.99	1.66	<0.034	23.88	0.054	1.05	1.75	1.07	9.17	3.29	41.02	17	88.29	20.62	229.34	53.21	0.237	102.52	0.000100181	0.82
MJ-02	86.39	3.77	<3.93	<0.209	0.097	308.29	0.79	<0.0257	13.39	<0.024	0.45	0.77	0.52	4.07	1.513	19.91	8.75	47.94	12.14	142.04	35.19	0.112	114.12	0.000122267	0.89
MJ-03	91.82	4.86	<3.55	<0.214	0.18	454.75	1.06	0.0218	16.37	0.075	0.96	1.26	0.79	6.88	2.395	29.89	12.94	68.74	16.99	196.33	47.3	0.158	56.38	7.50335E-05	0.82
MJ-04	168.76	7.5	<4.11	0.5	0.743	1142.93	2.05	0.467	31.51	0.239	3.45	5.06	2.49	23.14	7.78	91.28	35.47	172.72	39.23	417.14	89.53	0.361	21.83	0.00075652	0.70
MJ-05	158.61	10866.6	<2.91	0.29	3.55	1002.78	60.3	123.06	311.2	33.31	136	28.82	7.46	37.15	9.14	90.42	31.94	145.97	32.45	340.21	73.84	4.19	1.12	0.244430532	0.70
MJ-06	221.92	17.89	<3.44	0.215	0.484	1029.74	2.31	0.124	24.77	0.223	2.85	4.98	1.97	21.05	6.97	84	32.84	158.07	34.9	356.3	74.75	0.561	26.34	0.000235175	0.59
MJ-07	74.5	5.5	<3.96	0.51	1.113	321.22	0.89	0.077	12.37	0.033	0.51	1	0.58	4.95	1.815	22.34	9.68	49.81	12.08	137.87	32.08	0.168	57.36	0.000377404	0.79
MJ-08	139.36	9.22	<3.56	2.75	6.34	607.69	5.54	1.27	34.83	0.165	0.83	1.36	0.25	7.42	2.93	40.23	18.15	96.41	23.16	256.95	56.62	1.188	15.60	0.003339956	0.24
MJ-09	94.09	7.68	<3.99	<0.218	0.191	521.6	1.41	0.154	20.47	0.098	1.11	1.5	0.84	8	2.88	35.57	15.24	79.21	19.28	218.16	52.2	0.232	37.69	0.000477014	0.74
MJ-10	3178.4	4.08	<3.69	2.28	24.42	467.73	0.98	21.72	46.96	3.01	10.79	2.46	0.99	7.23	2.429	30.86	13.55	72.81	18.63	218.58	54.13	0.131	1.21	0.067148299	0.72
MJ-11	80.12	6.72	<4.64	<0.25	0.164	451.09	1.06	<0.033	15.61	0.04	0.82	1.22	0.71	6.5	2.24	29.94	13.03	70.32	17.54	200.27	48.02	0.16	85.42	0.000111348	0.77
MJ-12	140.88	7.69	<4.11	<0.242	0.193	831.15	2.07	0.036	30.5	0.093	1.46	2.71	1.4	13.62	5.04	61.76	25.37	127.15	29.11	313.71	70.3	0.357	82.04	7.75461E-05	0.70
MJ-13	159.1	512.98	<3.82	<0.242	0.166	702.79	1.94	0.03	16.05	0.16	2.93	4.36	1.71	16.78	5.35	60.32	22.76	105.87	23.02	232.02	47.95	0.382	26.84	8.73738E-05	0.61
MJ-14	143.98	12.51	<4.26	<0.25	0.167	698.51	1.89	0.023	26.12	0.1	1.5	2.87	1.16	13.56	4.71	56.34	22.05	105.63	23.8	244.44	51.74	0.436	68.87	6.3583E-05	0.57
MJ-15	105.4	6.97	<3.94	0.239	0.206	766.03	1.18	0.042	21.03	0.13	1.97	3	1.59	13.59	4.58	56.13	22.93	115.93	27.57	308	70.2	0.21	41.33	9.21476E-05	0.76
MJ-16	80.74	6.58	<2.80	<0.188	0.193	481.22	1.07	0.129	14.9	0.086	0.79	1.32	0.67	6.27	2.4	31.43	13.8	76.18	18.7	222.4	54.25	0.167	31.80	0.000391959	0.71
MJ-17	85.98	24.25	<4.76	<0.31	0.14	369.72	1.06	0.319	17.06	0.13	0.71	1.03	0.6	4.82	1.745	22.66	10.22	56.52	14.69	176.07	44.65	0.144	19.61	0.001224309	0.82
MJ-18	132.18	20.32	<5.12	<0.28	0.121	565.83	1.42	0.125	21.84	0.112	0.76	1.18	0.71	7.79	2.98	38.59	16.57	87.87	21.02	244.88	58.03	0.218	39.41	0.000344939	0.72
MJ-19	695.71	6.09	<4.65	<0.31	1.14	1322.69	1.44	1.234	36.01	0.483	5.94	7.2	3.71	26.17	8.23	94.98	38.06	194.72	46.49	512.64	118.08	0.178	10.93	0.001626628	0.83
MJ-20	132.91	8.74	<4.64	<0.33	0.133	600.61	1.37	0.047	16.6	0.094	1.17	1.9	0.83	8.8	3.26	41.96	18.2	94.03	22.73	258.4	61.09	0.271	42.61	0.000122911	0.62

All 20 analyses on zircon from sample XSZS have Th concentrations of 26.0 to 1160 ppm, U contents from 198 to 531 ppm, with Th/U ratios ranging from 0.43 to 0.85, showing typical magmatic characteristics. Concordant ages of 16 spots range from 124 ± 2 to 148 ± 2 Ma, with average $^{206}Pb/^{238}U$ age of 135.1 ± 3.3 Ma (95% confidence, MSWD=13) (Figure 5(b)). Their ages of $^{206}Pb/^{238}U$ can be divided into groups: older ages (mean 138.0 ± 2.5 Ma) and younger ages (mean 128.9 ± 3.3 Ma).

All 20 analyses on zircons from sample MJ have Th concentrations of 78.0 to 268 ppm, U concentrations of 84.78 to 242.26 ppm, with Th/U ratios ranging from 0.85 to 1.57, indicating magmatic origin. The $^{206}Pb/^{238}U$ apparent ages range from 129 ± 2 to 152 ± 3 Ma, with a weighted mean $^{206}Pb/^{238}U$ age of 137.3 ± 2.9 Ma (95% confidence, MSWD=7.5; Figure 5(c)). Similarly, these $^{206}Pb/^{238}U$ ages can be divided into two groups: older ages (mean 140.3 ± 2.9 Ma) and younger ages (mean of 132.2 ± 1.6 Ma). Two spots, MJ-20 and MJ-08, gave $^{206}Pb/^{238}U$ apparent ages of 194 ± 3 and 733 ± 7 Ma respectively. These two zircons have a core with heterogeneously spotted and estuary texture and an edge with weak oscillatory zoning. The $^{206}Pb/^{238}U$ apparent ages of 733 ± 7 Ma (MJ-08) are consistent with the $^{206}Pb/^{238}U$ apparent age of 731 ± 5 Ma (JGS-15), which is popular in the northern margin of the South China Block (Li *et al.* 2003; Sun *et al.* 2003; Zhou *et al.* 2006). It is obviously an inherited zircon from Neoproterozoic protoliths. MJ-05 spot show is disconcordant, indicating Pb loss.

Re–Os analytical results

Twelve pyrite samples selected from Xinqiao were analysed by the ICP-MS method (Table 3). The $^{187}Re/^{188}Os$ and $^{187}Os/^{188}Os$ values on the six samples by the ICP-MS method yield 5535 ± 258 to 29860 ± 1784 and 12.00 ± 1.04 to 65.11 ± 1.04 respectively. The isochron ages of six samples were calculated using the ISOPLOT software (Ludwig 2003) is 126 ± 11 Ma (Figure 6) with an initial Os ratio of 1.2 ± 1.9 (MSWD=2.6).

Major elements

The SiO_2 contents of the Tongling intrusive rocks vary from 53.6 to 64.1 wt-%. The total alkali contents vary from 5.4 to 8.5 wt-%, with K_2O contents ranging from 2.3 to 4.3%. Most samples of the Tongling intrusive rocks belong to high-K calc-alkaline series, two samples belong to shoshonitic series (Figure 7(a)).

In the Harker diagrams, several features are prominent: (1) high Al_2O_3 (>15.0 wt-%) and rich in Na ($Na_2O/K_2O>1.0$), with the exception of several samples (Figure 7(b) and (c)); (2) negative linear correlations between SiO_2 contents (from 54 to 64 wt-%) and those of TiO_2, CaO, MgO (Figure 7(d)–(f)), and P_2O_5 also shows the same behaviour as TiO_2, CaO and MgO (Figure 7(g)); and (3) no linear correlation between SiO_2 and Sr and Zr (Figure 7(h) and (i)).

The TiO_2, MgO, CaO, P_2O_5 contents of the Tongling intrusive rocks decrease linearly with increasing SiO_2 contents (Figure 7(d)–(g)), indicating that the magmas evolved from mafic- to intermediate-acid through fractional crystallization. However, K_2O, Al_2O_3, compatible element Zr and intermediate incompatible element Sr versus SiO_2 variation diagrams show that the intermediate-acid Tongling intrusive rocks were not simply derived from the fractional crystallization of a mafic magma (Figure 7(a), (b), (h) and (i)) (Wang *et al.* 2003b).

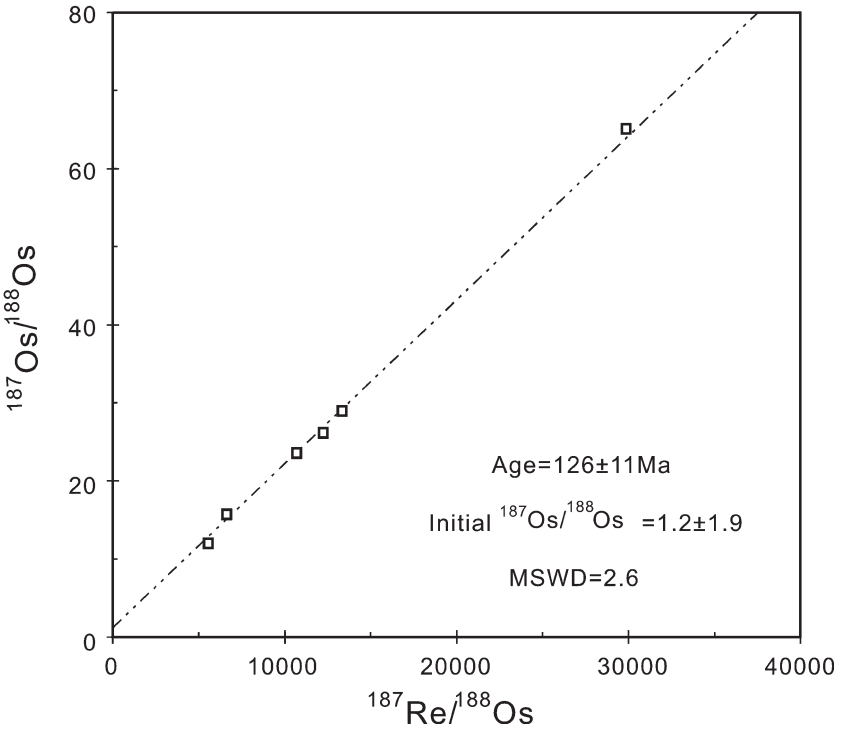

Figure 6. Re–Os isochron of pyrite in the Xinqiao deposit.

REE and trace elements

The total REE concentrations of the Tongling intrusive rocks (13 samples) range from 63.0 to 305 ppm, with a mean value of 161 ppm. All of the samples have the characteristics of LREE enrichment and HREE depletion without obvious Eu anomalies (Figure 8(a)). The chondrite-normalized REE patterns in the intermediate intrusive rocks from the Tongling area are very similar to those of the lower crust rocks (Rudnick *et al.* 2004). The LREE/HREE ratios vary from 8.60 to 12.4, with an average of 10.7, whereas the ratios of $(La/Yb)_N$ change from 7.87 to 17.0 (mean 12.1), showing strong LREE enrichment.

The chondrite normalized diagrams (Figure 8(b)) show consistent patterns for LILE, with positive Th, La, Ce anomalies, depletions in Nb, Ta, Zr, Hf and Ti, and a large range of Sr. By contrast, the transitional metal elements show patterns with depletions in Cr, Ni and positive Ti, Co (Figure 8(c)). Depletions in Nb, Ta, and Ti are typical characteristics of magmatic rock in a subduction zone, controlled by rutile (Kelemen 2003).

Rare earth elements and trace elements in zircon

The REE contents of zircons from JGS, MJ and XSZS samples are similar and display identical mantle normalized patterns (Figure 9). All are significantly enriched in heavy REE [$(La/Yb)_N<0.07$] and have positive Ce and negative Eu/Eu* anomalies. These features are generally consistent with the results given in prior literature for intermediate-acidic igneous rocks (Hoskin and Ireland 2000; Belousova *et al.* 2002).

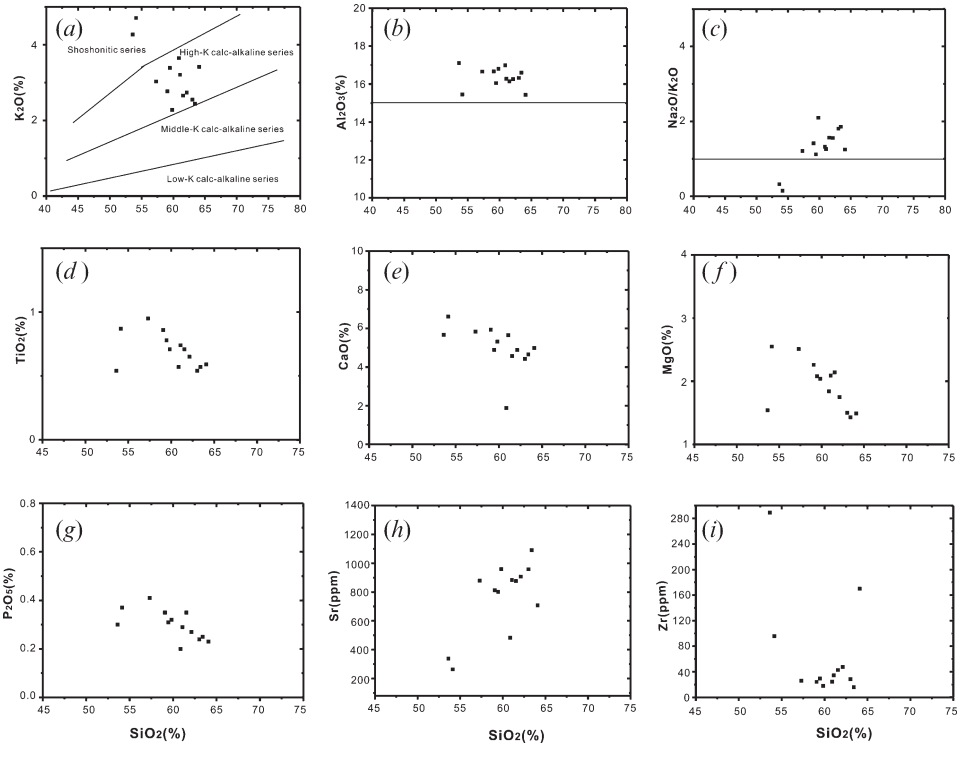

Figure 7. Harker variation diagrams for the intermediate intrusive rocks from Tongling area.

The Ce/Ce* and Eu/Eu* ratios were determined for all of the dated zircon grains as a measure of the oxidation state of the magma, but they are also temperature-dependent (Liang *et al.* 2006). The Ce/Ce* ratios of the JGS, XSZS and MJ can be divided into a high ratio group (>50) and a low ratio group (<50) (see Table 5). Eu anomalies are not distinct among JGS, XSZS and MJ.

Discussion

The formative age of the intermediate intrusive rocks

Zircon U–Pb ages by LA-ICP-MS yield two groups of 130–132 and 138–140 Ma for Jiguanshi quartz monzodiorite, Xishizishan quartz diorite and Miaojia diorite porphyry, respectively (Table 2; Figure 5). These ages represent two district magma activities within ~10 Ma in the Tongling region. The two concentrative magmatic intrusive events can supply abundant metal minerals. The older group is identical to previous dating results, within error, e.g. SHRIMP zircon U–Pb ages of 140.2 ± 2.2 Ma ($^{206}Pb/^{238}U$ age) and 138.9 ± 3.1 Ma for the Xinqiao and Xiaodongguanshan quartz diorites respectively (Wang *et al.* 2004a, b). These ages represent the formation age of these intermediate intrusive rocks. Interestingly, these ages are identical to former K–Ar and $^{40}Ar/^{39}Ar$ ages, ranging from 136.5 ± 0.9 to 138.6 ± 4.0 Ma and from 135.8 ± 1.1 to 137.3 ± 1.4 Ma, respectively (Chen *et al.* 1985; Zhou *et al.* 1987; Wu *et al.* 1996; Meng *et al.* 2004), as well as Rb–Sr, ranging from 135 to 137 Ma (Chen *et al.* 1993; Xing and Xu 1996). Given that the closure temperature of K–Ar and Rb–Sr isotopic systems are much lower than that of zircon, the identical ages of zircon and K–Ar and

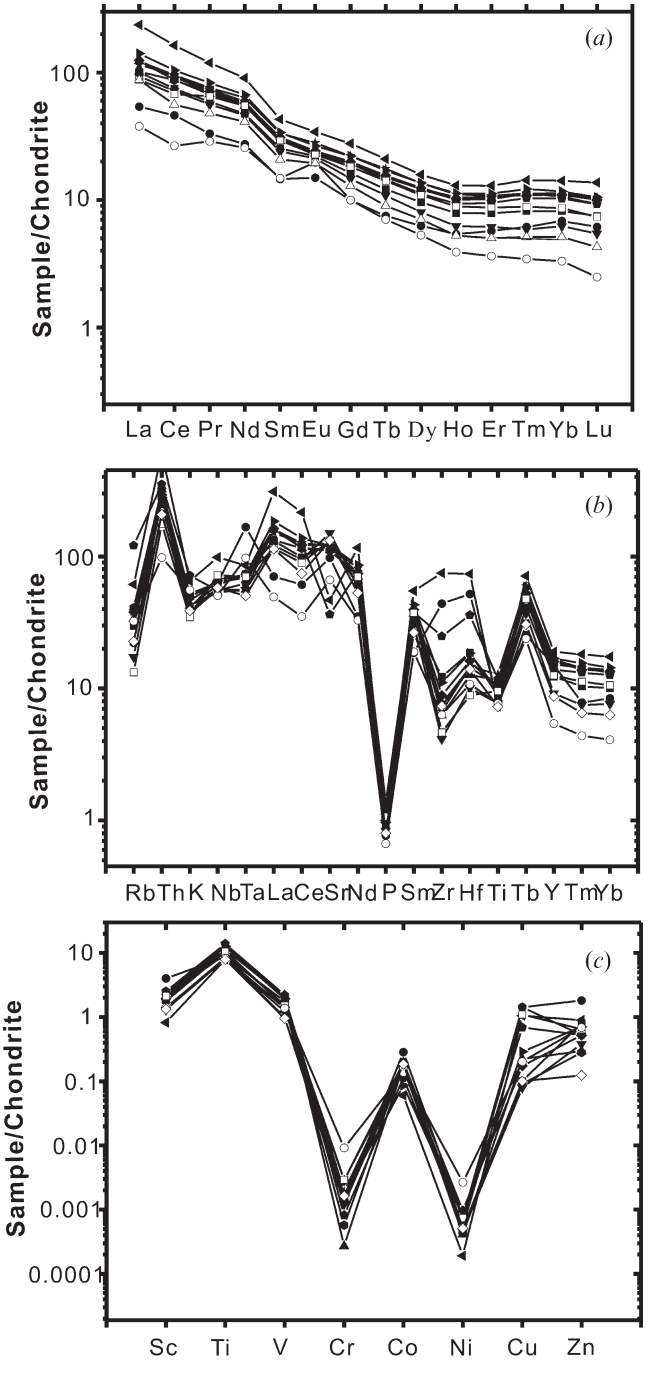

Figure 8. The rare earth elements patterns of the intermediate intrusive rocks from Tongling area: (a) and the trace element spider diagrams; (b, c) of the intermediate intrusion rocks in the Tongling area.

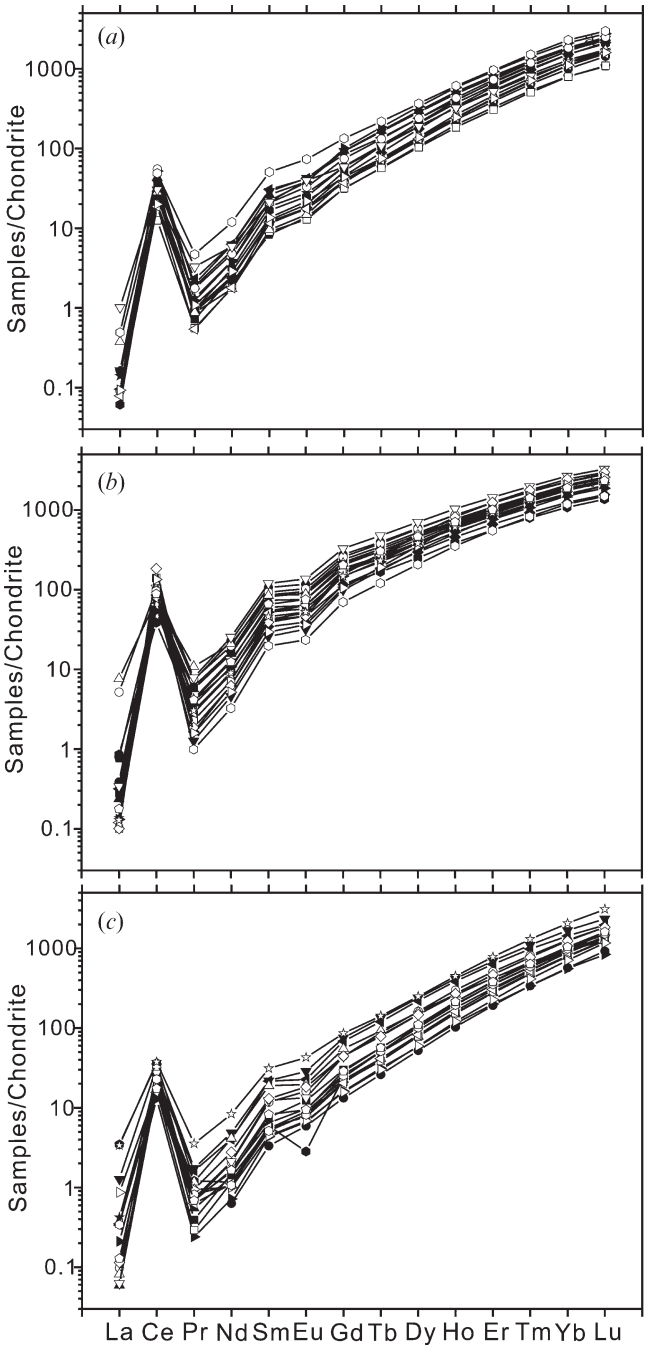

Figure 9. Zircon REE digrams of the intermediate intrusive rocks from Tongling area: (a) Jiguanshi quartz monzodiorite; (b) Xishizishan quartz diorite; (c) Miaojia diorite porphyry.

Rb–Sr indicate that either these intermediate intrusive rocks crystallized at temperatures below the closure temperature of K–Ar and Rb–Sr, or that these intrusive rocks experienced fast cooling right after formation or both. The closure temperature of K–Ar and Rb–Sr is 400–500°C, whereas the crystallization temperature

of Tongling intermediate intrusive rocks is 800°C. Therefore, the intermediate intrusive rocks experienced fast cooling during and/or immediately after crystallization.

Moreover, the formation ages of intermediate intrusive rocks are also identical to mineralization ages within error, e.g. molybdenite Re–Os, Os–Os ages of 138.0 ± 2.0 Ma for Longfushan golden ore deposits in the Shizhishan ore district (Sun *et al.* 2003), Re–Os isochron ages of 137.0 ± 0.2 and 138.6 ± 0.2 Ma from molybdenites of Jinkouling and Talimu Cu–Au ore deposits, respectively (Meng *et al.* 2004), and molybdenite Re–Os ages of 138.0 ± 3.2 to 140.8 ± 2.0 Ma (139 ± 3 Ma in average) and isochron age of 139.1 ± 2.7 Ma for stratiform skarn orebodies in the Datuanshan, Shatanjiao and Nanyangshan copper deposit (Mao *et al.* 2004).

The Rb–Sr pyrite isochron age of the Xinqiao deposit is 112.6 ± 7.8Ma (Wang *et al.* 2004a). We find that pyrite Re–Os has an Early Cretaceous isochron age of 126 ± 11 Ma from Xinqiao Cu–S–Fe ore deposit, representing the ore-forming age of iron-sulphide. This is close to albite $^{40}Ar/^{39}Ar$ age of 122.9 ± 0.2 to 124.9 ± 0.3 Ma from the Ningwu porphyry iron deposit 50 km away along the eastern part of the Yangtze metallogenic belt (Yu and Mao 2002). Thus there were at least two ore-forming events: one was closely related to copper and gold deposits (138–140 Ma), and the other was closely related to iron and sulphur deposits (120–126 Ma).

In Eu/Eu* versus $^{206}Pb/^{238}U$ age diagram (Figure 10), these zircon samples from three intrusive rocks (JGS, XSZS and MJ) show a sinusoid or cosine curve trend. The Eu/Eu* values naturally divide into one group of 0.6 to 0.7 and another group of 0.7 to 0.9. In Ce/Ce* versus $^{206}Pb/^{238}U$ age diagram (Figure 11), these zircon samples from the JGS intrusive rock show a sinusoid or cosine curve trend with a peak value at about 130 and 139 Ma and vale value at about 126 and 134 Ma (Figure 11(a)). The peak value age is just consistent with the two group ages. The zircon samples from the XSZS intrusive rock have two variational trends: one that shows a sinusoid or cosine curve trend in low Ce anomalies (<50) and another that shows a sinusoid or cosine curve trend in high Ce anomalies (>100) (Figure 11(b)). The zircon samples from the MJ intrusive rock show a sinusoid or cosine curve trend that is similar to the samples from the JGS intrusive rock (Figure 11(c)). The Ce and Eu particular anomaly characteristics for three intermediate intrusive rocks show at least two hydrothermal fluids with high Ce anomaly fluid and low Ce anomaly fluid. The zircon Ce anomaly is controlled mainly by the oxygen fugacity of the magma and, to a lesser extent, by the temperature of crystallization (Bedard 1999). Empirical associations suggest that oxygen fugacity is the dominant effect given that the link between oxidized felsic magmas and mineralization is well known (Hedenquist and Lowenstern 1994; Ballard *et al.* 2002; Sun *et al.* 2004). The oxygen fugacity of magmas controls the oxidation state of sulphur in a melt: at low oxygen fugacity, sulphur in the magma exists mainly as S^{2-}, whereas at high oxygen fugacity, it exists mainly as SO and SO_2. The transition of S^{2-} to SO or SO_2 may prevent the saturation of an immiscible sulphide phase that scavenges Cu from a fractionating melt (Sun *et al.* 2004). Copper in magma with high oxygen fugacity will then become enriched during differentiation and partition into a magmatic-hydrothermal fluid (Cline and Bodnar 1991; Pasteris 1996; Ulrich *et al.* 1999; Ballard *et al.* 2002; Sun *et al.* 2004). The high Ce anomaly is closely related with copper and gold, while the low Ce anomaly is closely related with iron and sulphur. This is consistent with the two ore-forming ages: molybdenite Re–Os age (138–140 Ma) related with copper and gold ore deposits and pyrite Re–Os age (126 ± 11 Ma) related with iron and sulphur ore deposits.

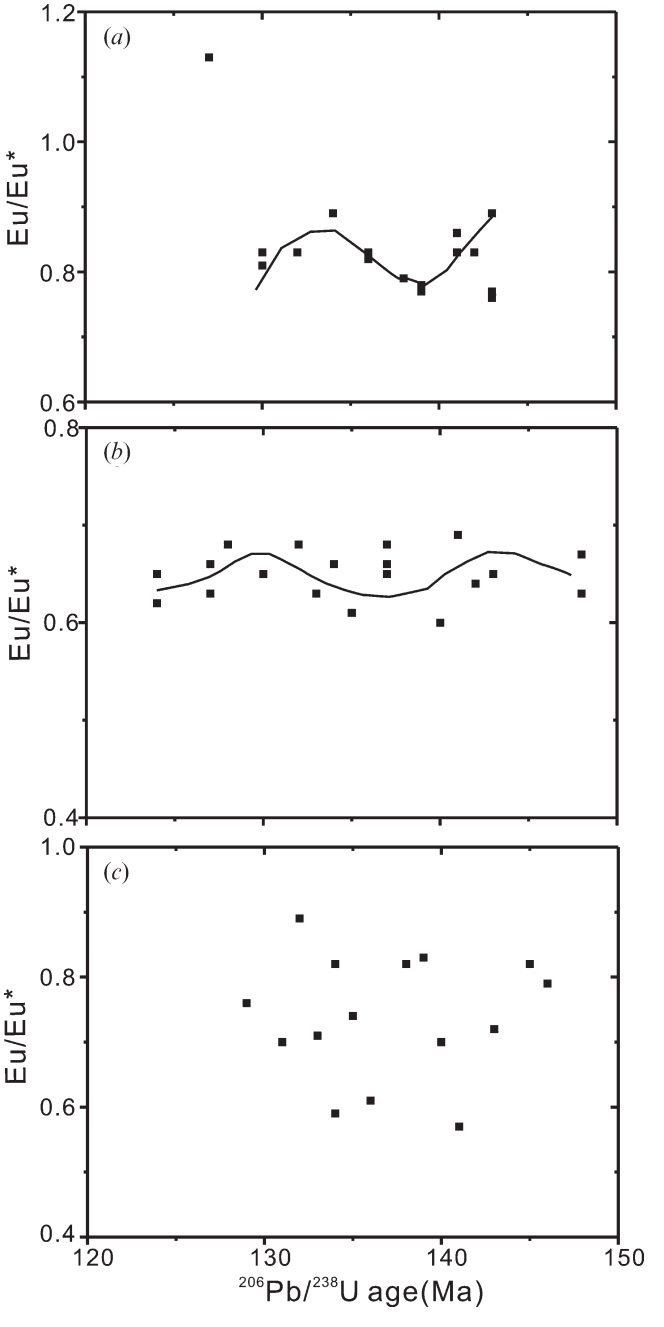

Figure 10. Eu/Eu*–$^{206}Pb/^{238}U$ age diagrams of the intermediate intrusive rocks in Tongling region: (a) Jiguanshi quartz monzodiorite; (b) Xishizishan quartz diorite; (c) Miaojia diorite porphyry.

Dynamic setting of rock- and ore-formations

The intermediate intrusive rocks of the Tongling area show trace element patterns of depletions in HFSE, e.g. Nb, Ta, Zr, Hf, Ti, and enrichments in LILE, e.g. Th, La, Ce (Figure 8(b)), similar to convergent margin magmas. Depletions in Nb, Ta, and

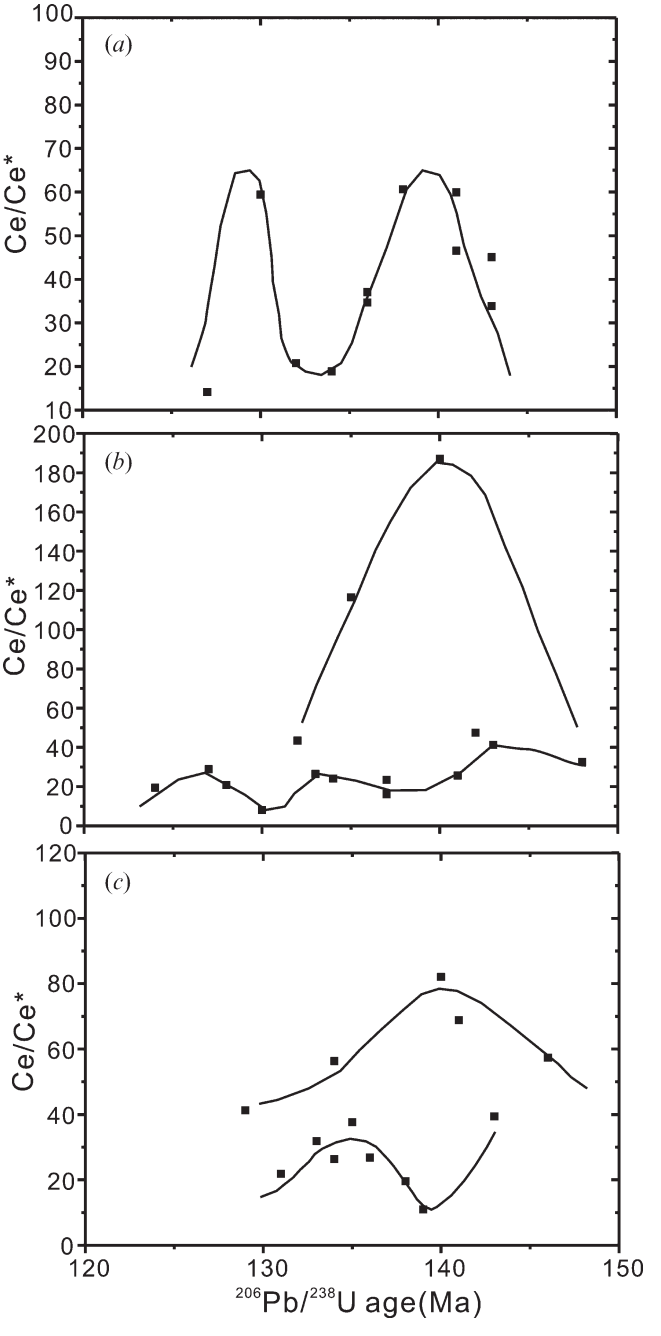

Figure 11. Ce/Ce*–$^{206}Pb/^{238}U$ age diagrams of the intermediate intrusive rocks in Tongling region: (a) Jiguanshi quartz monzodiorite; (b) Xishizishan quartz diorite; (c) Miaojia diorite porphyry.

Ti are typical characteristics of magmatic rock in subduction zones. These characteristics are different from intra plate igneous rocks, which usually show enrichments in high field strength elements.

The main form of crust-mantle interaction in a subduction zone is dehydration of the subduction slab, forming the fluid enriched LILE that emplaced overturn mantle wedge. Partial melting of the mantle wedge forms island arc magmatic rock. Partial melting of the subduction slab could form adakite magma. Some geochemical characteristics of the ore-bearing intermediate intrusive rocks are consistent with those of adakite, e.g. Al_2O_3 >15 wt-%, low HREE (Yb <1.9 ppm) and Y (<18 ppm) contents, high Sr (>400 ppm) content and Sr/Y ratio >20, and positive Sr and Eu anomalies (Defant and Drummond 1990). The Nb/Ta and Pb/Nd ratios are also consistent with those of adakite (Table 4) (Kamber *et al.* 2002). In a Sr/Y versus Y diagram (Figure 12(a)), all samples show a negative correlation trend. Both values of Sr/Y and Y values vary dramatically. Remarkably, only one sample plotted in the adakite field; most of the samples plotted in the arc volcanic rock field, with a few samples plotting between the adakite field and arc volcanic rock field. This implies

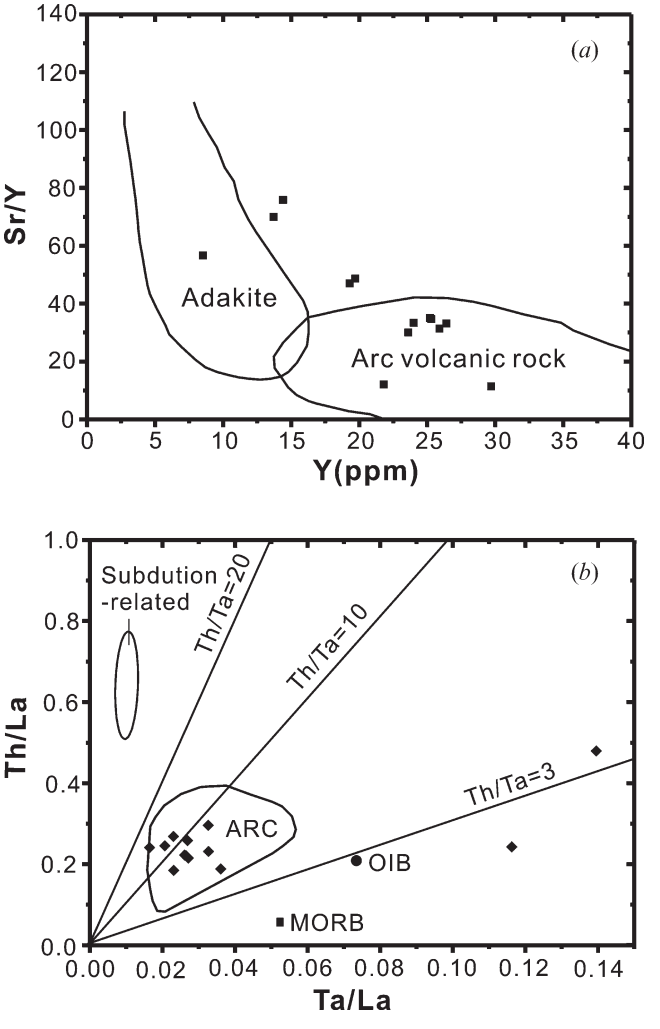

Figure 12. Trace element ratio diagrams of the intermediate intrusive rocks in the Tongling region: (a) Sr/Y–Y diagram (Kepezhinskas *et al.* 1997); (b) Th/La–Ta/La diagram (Kay and Gordollo 1994).

that intermediate intrusive rocks in the Tongling region were likely formed through magma mixing of more than two compositional end-members. This is consistent with the major elements results. In a Th/La versus Ta/La diagram (Figure 12(b)), most samples are also plotted in ARC field, with Th/Ta from 3 to 20. Only two samples are plotted in the above Th/Ta=20 field, while one sample is plotted in the below Th/Ta=3 field. The Ta/La ratios cover a large range, with much less variation in Th/La ratios. Figure 12 reflects that ARC was the primary environment of rock-forming in the Tongling region.

In an Rb versus Y+Nb diagram, all samples plot in or near VAG (Figure 13). Previous studies indicate arc-magma rocks have a polarity of compositions (Sakuyama and Nesbitt 1986; Wilson 1989). Through the area, the alkalinity of magma rocks increases from trench to inland; over time, the alkalinity of the assemblage of magma rocks as a whole increases. Compositions of magma rocks in active continental margin were the main characteristics of high-potassium (Wilson 1989). The geochemical characteristics of magmatic rocks from the Tongling area quite clearly indicate that the tectonic setting of Yanshanian igneous rocks should be to the side of arc-magmatic inland in active continental margin closely related to subduction of the Pacific plate, tending towards back-arc environment to late time (Lu *et al.* 2005). These findings are consistent with those of many investigators (Jahn 1974; Holloway 1982; Zhou and Li 2000; Sun *et al.* 2007).

Significance of ore-forming

The firestorm of volcano-magma was an earthshaking geological event within the Yanshanian movement in eastern China. Such large-scale Yanshanian magmatic activity was a major cycle of the matter of crust-mantle and a major transfer of physical energy, resulting in the most characteristic ore-forming event in Chinese geological history.

Previous studies (Bedard 1999; Seghedi *et al.* 2001) indicated that Ba is the most mobile incompatible element in arc magmatism caused by fluids released from the subducted slab, whereas Th is preferentially enriched in melts derived from the subducted slab. The Ba–Nb/Y diagram (Figure 14(a)) shows that both Ba contents

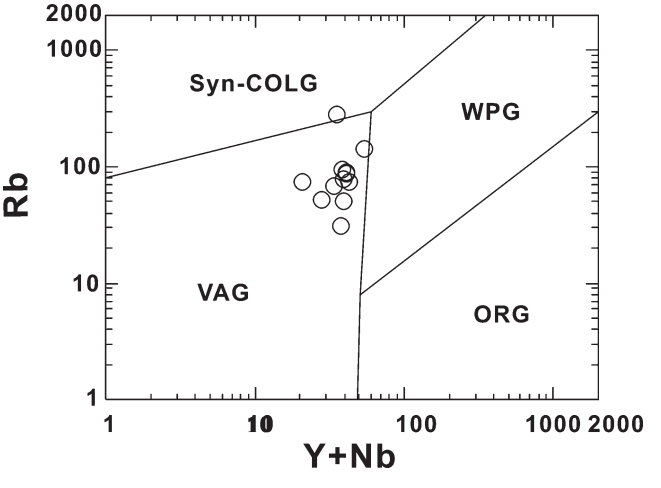

Figure 13. Tectonic discrimination diagrams for the intermediate intrusive rocks from Tongling area (Pearce *et al.* 1984).

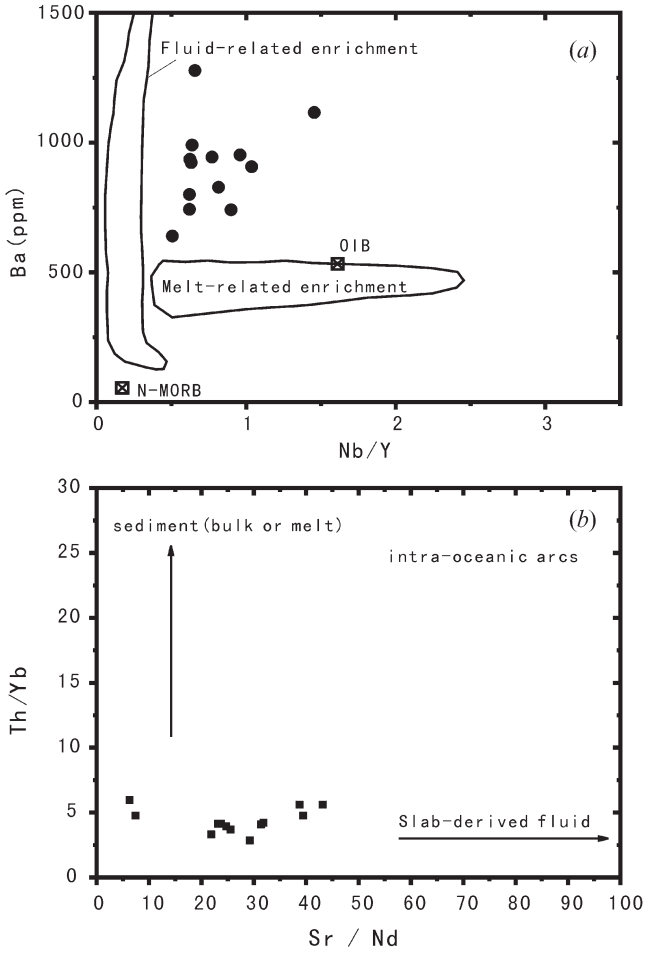

Figure 14. Trace element ratio diagrams of the intermediate intrusive rocks in the Tongling region: (a) Ba–Nb/Y diagram (Kepezhinskas *et al.* 1997); (b) Th/Yb–Sr/Nd diagram (Woodhead *et al.* 1998).

and Nb/Y ratios of intermediate intrusive rocks are quite centralized. In the Ba–Nb/Y diagram, nearly all samples plot in between fluid-related enrichment and melt-related enrichment, showing that neither fluid-related enrichment nor melt-related enrichment singly controlled the metal sources of the ore-bearing intrusive rocks in the Tongling region. It is possible that the overprinting of melt-related enrichment and fluid-related enrichment resulted in a unique ore-forming condition in the Tongling area. In the Th/Yb–Sr/Nd diagram (Figure 14(b)), the ratios of Th/Yb are fairly concentrated around a mean of about five, while the Sr/Nd ratios have a large range. Only one sample plots in the sediment (bulk or melt) development line; the other samples all plot near the origination place of the sediment (bulk or melt) development line and slab-derived fluid, indicating that there was no single metal source of the ore-bearing intrusive rocks.

A large number of studies suggested that large-scale copper (gold) metallogenesis is usually closely associated with convergent margin magmas (Richards 1990;

Mueller and Groves 1993; Sillitoe 1997; Ulrich *et al.* 1999), but formation of the copper–gold deposits ores are mainly determined by the nature of melting, fluid and wall rock (McInnes *et al.* 1999; Mueller *et al.* 2001; Sun *et al.* 2004; Levresse *et al.* 2006; Niiranen *et al.* 2007). Most of the world's copper–gold (Cu–Au) ore deposits (e.g. epithermal/porphyry types) are associated with convergent margin magmas, usually characterized by a high fO_2 (Sillitoe 1997; Mungall 2002; Sun *et al.* 2004).

These ore metals might ultimately have been recycled from the subducted slab. Partial melting of the subducted slab might produce adakitic melting or, under high temperature and pressure conditions, the subducted slab released high fo_2 aqueous supercritical fluid enriched Fe_2O_3, and melting of the mantle wedge formed mother magmas enriched volatilizations (S and so on) and ore-forming elements (Cu, Au and so on). The mixing of the mother magmas and the crustal matters released Cu, Au-bearing epithermal. This ore metal-bearing epithermal ultimately formed ore deposits, while corresponding magmatic rock associations are often accompanied by rocks of alkaline series and shoshonitic series. Based on the geochemical and geochronological characteristics of intermediate intrusive rocks in Tongling area, the Early Cretaceous period magmatic activity and related metallogenesis is closely related to subduction of the Pacific plate.

Conclusions

(1) Laser ablation ICP-MS U–Pb of zircons dating yielded two group ages (about 130–132 and 138–140 Ma) for the Jiguanshi quartz monzodiorite, Xishizishan quartz diorite and Miaojia diorite porphyry, which are the most important magmatic rocks in the Tongling area related to Cu–Au deposits. Based on other high-precision dating ages of intrusive rocks and mineralization deposits, we obtained pyrite Re–Os age from the Xinqiao ore deposit. Characteristics of trace elements of zircon show that one ore-forming event with high Ce abnormality happened at molybdenite Re–Os age (138–140 Ma) and was related to copper and gold ore deposit, and another ore-forming event with low Ce abnormality happened at pyrite Re–Os age (126 ± 11 Ma) and was related to iron and sulphur ore deposits in the Tongling region.

(2) The Tongling intermediate intrusive rocks are mainly high-K calc-alkaline series and shoshonitic series. Some geochemical characteristics of the intermediate intrusive rocks are consistent with those of adakite.

(3) The Tongling intrusive rocks are a magma mixture of more than two compositional end-members; the mixing of mantle-derived and crust-derived magmas might have been the main mechanism through which the Tongling intrusive rocks were produced.

(4) The geochemical and geochronological characteristics of intermediate intrusive rocks in Tongling region show the Early Cretaceous period magmatic activity related regional Cu–Au metallogenesis, which are possibly due to the subduction of the Pacific plate.

Acknowledgements

This study is supported by Chinese Ministry of Science and Technology (2006CB403505), the Knowledge Innovation Project of Chinese Academy of Sciences (KZCX1-YW-15-3) and NSF (No. 40525010). Professor Yinfo Chang is highly appreciated for constructive suggestions, Miss Elaine Chang improved the manuscript.

References

Andersen, T., 2002, Correction of common lead in U–Pb analyses that do not report ^{204}Pb: Chemical Geology, v. 192, p. 59–79.

Anom, A.B.M., 1987, The Regional Geology of Anhui Province: Beijing, Geological Publishing House, p. 1–721.

Ballard, J.R., Palin, J.M., and Campbell, I.H., 2002, Relative oxidation states of magmas inferred from Ce(IV)/Ce(III) in zircon: Application to porphyry copper deposits of northern Chile: Contributions to Mineralogy and Petrology, v. 144, p. 347–364.

Bedard, J.A., 1999, Petrogenesis of boninites from the Betts Cove ophiolite, New foundland, Canada: Identification of subducted source components: Journal of Petrology, v. 40, p. 1853–1889.

Belousova, E.A., Griffin, W.L., Suzanne, Y.O.R., and Fisher, N.I., 2002, Igneous zircon: Trace element composition as an indicator of source rock type: Contributions to Mineralogy and Petrology, v. 143, no. 5, p. 602–622.

Chang, Y.F., Liu, X.P., and Wu, Y.C., 1991, The Copper–Iron Belt of the Middle and Lower Reaches of the Changjiang River: Beijing, Geological Publishing House, p. 1–379.

Chen, J.F., Foland, K.A., and Zhou, T.X., 1985, Mesozoic granitiods of the Yangtze fold belt, China: Isotopic constrains on the magma sources, *in* Wu, L.R. et al., The crust – the significance of granites gneisses in lithosphere: Athens, Theophrastus, p. 217–237.

Chen, J.F., Zhou, T.X., Li, X.M., Foland, K.A., Huang, C.Y., and Lu, W., 1993, Sr and Nd isotopic constraints on source regions of the intermediate and acidic intrusions from southern Anhui Province: Geochimica, v. 22, no. 3, p. 26 l–268.

Chen, J.F., and Jahn, B.M., 1998, Crustal evolution of Southeastern China: Nb and Sr isotopic evidence: Tectonophysics, v. 284, p. 101–133.

Cline, J.S., and Bodnar, R.J., 1991, Can economic porphyry copper mineralization be generated by a typical calc-alkaline melt?: Journal of Geophysical Research, v. 96, p. 8113–8126.

Defant, M.J., and Drummond, M.S., 1990, Derivation of some modern arc magmas by melting of young subducted lithosphere: Nature, v. 347, p. 662–665.

Deng, J.F., Dai, S.Q., Zhao, H.L., and Du, J.G., 2002, Recognition of magma-fluid-metallogenic system and subsystem in the Tongling Cu–Au (Ag) metallogenic area: Mineral Deposits, v. 21, no. 4, p. 317–322.

Deng, J.F., and Wu, Z.X., 2001, The thinning of lithosphere of the lower Yangtze craton and Cu–Fe metallogenic zone of middle-lower reaches: Anhui Geology, v. 11, no. 2, p. 86–91, (in Chinese with English abstract).

Du, A.D., He, H.L., Yin, N.W., Zou, X.Q., Sun, Y.L., Sun, D.Z., Chen, S.Z., and Qu, W.J., 1994, A study on the rhenium-osmium geochronometry of molybdenites: Acta Geologica Sinica, v. 38, p. 339–347.

Du, Y.S., and Li, X.J., 1997, The study of enclaves and the discussion of magmatic-metallogenic processes in the typical diggings of Tongling area, Anhui Province: Geological Journal of China Universities, v. 3, no. 2, p. 171–172, (in Chinese with English abstract).

Gao, S., Liu, X.M., Yuan, H.L., Hattendorf, B., Günther, D., Chen, L., and Hu, S.H., 2002, Determination of forty-two major and trace elements of USGS and NIST SRM glasses by LA-ICPMS: Geostandard Newsletters, v. 26, p. 181–195.

Guillong, M., Horn, I., and Günther, D., 2003, A comparison of 266 nm, 213 nm and 193 nm produced from a single solid state Nd: YAG laser for laser ablation ICP-MS: Journal of Analytical Atomic Spectrometry, v. 18, p. 1224–1230.

Guo, W.K., 1982, On granitoid and metallogenesis: Regional Geology of China, no. 2, p. 15–30.

Hedenquist, J.W., and Lowenstern, J.B., 1994, The role of magmas in the formation of hydrothermal ore deposits: Nature, v. 370, p. 519–527.

Holloway, N.H., 1982, North Palawan Block, Philippines – Its relation to Asian mainland and role in evolution of South China Sea: American Association of Petroleum Geologists Bulletin, v. 66, p. 1355–1383.

Hoskin, P.W.O., and Ireland, T.R., 2000, Rare earth element chemistry of zircon and its use as a provenance indicator: Geology, v. 28, p. 627–630.

Jahn, B.M., 1974, Mesozoic thermal events in southeast China: Nature, v. 248, p. 480–483.

Kamber, B.S., Evart, A., Collerson, K.D., Bruce, M.C., and McDonald, G.D., 2002, Fluid-mobile trace element constraints on the role of slab melting and implications for Archaean crustal growth modals: Contributions to Mineralogy and Petrology, v. 144, p. 38–56.

Kay, S.M., and Gordollo, C.E., 1994, Pocho volcanic rocks and the melting of depleted continental lithosphere above a shallowly dipping subduction zone in the central Andes: Contributions to Mineralogy and Petrology, v. 117, p. 25–44.

Kelemen, P., 2003, One view of the geochemistry of subduction-related magmatic arcs with emphasis on primitive andesite and lower crust., *in* Holland, H.D., and Turekian, K.K., eds., Treatise on geochemistry: Amsterdan, Elsevier, p. 612–615.

Kepezhinskas, P., McDermott, F., Defant, M.J., Hochstaedter, A., Drummond, M.S., Hawkesworth, C.J., Koloskov, A., Maury, R.C., and Bellon, J., 1997, Trace element and Sr–Nd–Pb isotopic constraints on a three-component model of Kammchatka Arc petrogenesis: Geochimica et Cosmochimica Acta, v. 61, p. 577–600.

Levresse, G., Tritlla, J., Villareal, J., and Gonzalez-Partida, E., 2006, The "El Pilote" fluorite skarn: A crucial deposit in the understanding and interpretation of the origin and mobilization from northern Mexico deposits: Journal of Geochemical Exploration, v. 89, p. 205–209.

Liang, H.-Y., Campbell, I.H., Allen, C., Sun, W.-D., Liu, C.-Q., Yu, H.-X., Xie, Y.-W., and Zhang, Y.-Q., 2006, Zircon Ce^{4+}/Ce^{3+} ratios and ages for Yulong ore-bearing porphyries in eastern Tibet: Mineralium Deposita, v. 41, p. 152–159.

Li, W.D., Mao, J.R., and Zhu, Y.H., 1998, The Mesozoic igneous rocks and mineral deposits in southeastern China: Beijing, Seismological Press, 159 p.

Li, X.H., Li, Z.X., Ge, W., Zhou, H., Li, W., Liu, Y., and Wingate, M.T.D., 2003, Neoproterozoic granitoids in South China: Crustal melting above a mantle plume at ca. 825 Ma?: Precambrian Research, v. 122, p. 45–83.

Lu, Q.T., Hou, Z.Q., Yang, Z.S., and Shi, D.N., 2005, Underplating in the middle-lower Yangtze Valley and model of geodynamic evolution: Constraints from geophysical data: Science in China Series D-Earth Sciences, v. 48, no. 7, p. 985–999.

Ludwig, K.R., 2003, ISOPLOT 3.00: a geochronological toolkit for Microsoft Excel: Berkeley Geochronology Center Special Publication No. 4, p. 1–70.

Mao, J.R., Su, Y.X., and Chen, S.Y., 1990, The intermediate-aced intrusive rocks and mineralization in the Middle-lower Reaches of the Yangtze River: Beijing, Geological Publishing House, p. 1–191, (in Chinese with English abstract).

Mao, J.W., Holly, S., Du, A.D., Zhou, T.F., Mei, Y.X., Li, Y.F., Zang, W.S., and Li, J.W., 2004, Molybdenite Re–Os precise dating for molybdenite from Cu–Au–Mo deposits in the Middle-Lower Reaches of Yangtze River belt and its implications for mineralization: Acta Geologica Sinica, v. 78, no. 1, p. 121–131.

McInnes, B.I.A., McBride, J.S., Evans, N.J., Lambert, D.D., and Andrew, A.S., 1999, Osmium isotope constraints on ore metal recycling in subduction zones: Science, v. 286, p. 512–516.

Meng, Y.F., Yang, Z.S., Zeng, P.S., Xu, W.Y., and Wang, X.C., 2004, Tentative temporal constraints of ore-forming fluid systems in Tongling metallogenic province: Mineral Deposits, v. 23, no. 3, p. 271–280, (in Chinese with English abstract).

Mueller, D., Franz, L., Herzig, P.M., and Hunt, S., 2001, Potassic igneous rocks from the vicinity of epithermal gold mineralization, Lihir Island, Papua New Guinea: Lithos, v. 57, p. 163–186.

Mueller, D., and Groves, D.I., 1993, Direct and indirect associations between potassic igneous rocks, shoshonites and gold–copper deposits: Ore Geology Reviews, v. 8, p. 383–406.

Mungall, J.E., 2002, Roasting the mantle: Slab melting and the genesis of major Au and Au-rich Cu deposits: Geology, v. 30, p. 915–918.

Niiranen, T., Poutiainen, M., and Mänttäri, I., 2007, Geology, geochemistry, fluid inclusion characteristics, and U–Pb age studies on iron oxide–Cu–Au deposits in the Kolari region, northern Finland: Ore Geology Reviews, v. 30, p. 75–105.

Pan, Y.M., and Dong, P., 1999, The Lower Changjiang (Yangzi/Yangtze River) metallogenic belt, east central China: intrusion- and wall rock-hosted Cu–Fe–Au, Mo, Zn, Pb, Ag deposits: Ore Geology Reviews, v. 15, no. 4, p. 177–242.

Pasteris, J.D., 1996, Mount Pinatubo volcano and "negative" porphyry copper deposits: Geology, v. 24, p. 1075–1078.

Pearce, J.A., Harris, N.B.W., and Tindle, A.G., 1984, Trace element discrimination diagrams for the tectonic interpretation of granitic rocks: Journal of Petrology, v. 25, p. 956–983.

Richards, J.P., 1990, Petrology and geochemistry of alkaline intrusives at the Porgera gold deposit, Papua New Guinea: Journal of Geochemical Exploration, v. 35, p. 141–199.

Rudnick, R.L., Gao, S., Ling, W.L., Liu, Y.S., and McDonough, W.F., 2004, Petrology and geochemistry of spinel peridotite xenoliths from Hannuoba and Qixia, North China craton: Lithos, v. 77, p. 609–637.

Sakuyama, M., and Nesbitt, R.W., 1986, Geochemistry of Quaternary volcanic rocks of the northeast Japan arc: Journal of Volcanology and Geothermal Research, v. 29, p. 413–450.

Seghedi, I., Downes, H., Pecskay, Z., Thirlwall, M.F., Szakas, A., Prychodko, M., and Mattey, D., 2001, Magmagenesis in a subduction-related post-collisional volcanic arc segment: the Ukrainian Carpathians: Lithos, v. 57, p. 237–262.

Sillitoe, R.H., 1997, Characteristics and controls of the largest porphyry Cu–Au and epithermal Au deposits in the circum-Pacific region: Australian Journal of Earth Sciences, v. 44, p. 373–388.

Smoliar, M.I., Walker, R.J., and Morgan, J.W., 1996, Re–Os ages of group IIA, IIIA, IVA and VIB iron meteorites: Science, v. 271, p. 1099–1102.

Sun, W.D., Arculus, R.J., Kamenetsky, V.S., and Binns, R.A., 2004, Release of gold-bearing fluids in convergent margin magmas prompted by magnetite crystallization: Nature, v. 431, p. 976–978.

Sun, W.D., Ding, X., Hu, Y.H., and Li, X.H., 2007, The golden transformation of the Cretaceous plate subduction in the west Pacific: Earth and Planetary Science Letters, v. 262, no. 3–4, p. 533–542.

Sun, W.D., Xie, Z., Chen, J.F., Zhang, X., Chai, Z.F., Du, A.D., Zhao, J.S., Zhang, C.H., and Zhou, T.F., 2003, Os–Os Dating of copper and molybdenum deposits along the Middle and Lower Reaches of Yangtze River, China: Economic Geology, v. 98, no. 1, p. 175–180.

Tang, Y.C., Wu, Y.C., Chu, G.Z., Xing, F.M., Wang, Y.M., Cao, F.Y., and Chang, Y.F., 1998, Geology of copper-gold polymetallic deposits along the Yangtze River, Anhui Province: Beijing, Geological Publishing House, p. 1–351.

Ulrich, T., Guether, D., and Heinrich, C.A., 1999, Gold concentrations of magmatic brines and the metal budget of porphyry copper deposits: Nature, v. 399, p. 676–679.

Wang, Q., Xu, J.F., Zhao, Z.H., Xiong, X.L., and Bao, Z.W., 2003a, Petrogenesis of the Mesozoic intrusive rocks in the Tongling area, Anhui Province, China and their constraint on geodynamic process: Science in China Series D-Earth Sciences, v. 46, no. 8, p. 801–815.

Wang, Q., Zhao, Z.H., Xu, J.F., Li, X.H., Bao, Z.W., Xiong, X.L., and Liu, Y.M., 2003b, Petrogenesis and metallogenesis of the Yanshanian adakite-like rocks in the Eastern Yangtze block: Science in China (Series D), v. 46(supp.), p. 164–176.

Wang, X.L., Zhou, J.C., Qiu, J.S., Zhang, W.L., Liu, X.M., and Zhang, G.L., 2006, LA-ICP-MS U–Pb zircon geochronology of the Neoproterozoic igneous rocks from Northern Guangxi, South China: Implications for tectonic evolution: Precambrian Research, v. 145, p. 111–130.

Wang, Y.B., Liu, D.Y., Meng, Y.F., Zeng, P.S., Yang, Z.S., and Tian, S.H., 2004a, SHRIMP U–Pb geochronology of Xiaodongguanshan quartz-dioritic intrusions in Tongling

district and its petrogenetic implications: Acta Petrologica et Mineralogica, v. 23, no. 4, p. 298–304, (in Chinese with English abstract).

Wang, Y.B., Liu, D.Y., Zeng, P.S., Yang, Z.S., Meng, Y.F., and Tian, S.H., 2004b, Rb–Sr dating the pyrite of the Xinqiao Cu–S–Fe–Au deposit, Tongling, Anhui Province: Geological Review, v. 50, no. 9, p. 538–542, (in Chinese with English abstract).

Wang, Y.L., Wang, Y., Zhang, Q., Jia, X.Q., and Han, S., 2004c, The geochemical characteristics of Mesozoic intermediate-acid intrusives of the Tongling area and its metallogenesis-geodynamic implications: Acta Petrologica Sinica, v. 20, no. 2, p. 325–338.

Weng, W.H., 1920, On regional distribution of deposits in China: Geological Report, v. 2, p. 9–21.

Wilson, M., 1989, Igneous petrogenesis: a global tectonic approach: London, Unwin and Hyman, p. 1–466.

Woodhead, J.D., Eggins, S.M., and Johnson, R.W., 1998, Magma genesis in the New Britain island arc: Further insights into melting and mass transfer processes: Journal of Petrology, v. 39, p. 1641–1668.

Wu, C.L., Chen, S.N., Shi, R.D., and Hao, M.Y., 2003, Origin and features of the Mesozoic intermediate-acid intrusive rocks in the Tongling area, Anhui, China: Acta Geoscientia Sinica, v. 24, no. 1, p. 41–48.

Wu, C.L., Wang, F.S., Hao, M.Y., and Shi, R.D., 2000, Geochronology of intermediate-Acid Intrusive Rocks from Tongling, Anhui: Continental Dynamics, v. 5, no. 1, p. 15–23.

Wu, C.L., Zhou, X.R., Huang, X.C., Zhang, C.H., and Huang, W.M., 1996, Geochronology of intermediate-acid intrustive rocks from Tongling district: Acta Petrologica et Mineralogica, v. 15, no. 4, p. 299–306.

Xie, J.C., Yang, X.Y., Du, J.G., and Sun, W.D., 2008, Zircon U–Pb geochronology of the Mesozoic intrusive rocks in the Tongling region: Implications for copper–gold mineralization: Acta Petrologica Sinica, v. 24, p. 1782–1800, (in Chinese with English abstract).

Xing, F.M., and Xu, X., 1999, Yangtze Magmatic Belt and Metallogenesis: Hefei, Anhui People's Pubulishing House, p. 1–170.

Xing, F.M., 1998, The geochemistry of mafic rocks in the east of Yangtze magmatic belt: Geochimica, v. 27, no. 3, p. 258–268.

Xing, F.M., and Xu, X., 1995, The essential features of mamatic rocks along the Yangtze River in Anhui Province: Acta Petrologica Sinica, v. 11, p. 409–420, (in Chinese with English abstract).

———, 1996, High-potassisum calc-alkaline intrusive rocks in Tongling area, Anhui Province: Geochimica, v. 25, no. 1, p. 29–38.

Xu, G., and Lin, X., 2000, Geology and geochemistry of the Changlongshan skarn iron deposit, Anhui Province, China: Ore Geology Reviews, v. 16, no. 1–2, p. 91–106.

Xu, G., and Zhou, J., 2001, The Xinqiao Cu–S–Fe–Au deposit in the Tongling mineral district, China: Synorogenic remobilization of a stratiform sulphide deposit: Ore Geology Reviews, v. 18, no. 1–2, p. 77–94.

Yang, X.M., and Lin, W.T., 1988, The study of petrogenesis mechanism of Tongguanshan igneous complex: Geological Review, v. 34, no. 1, p. 25–35, (in Chinese with English abstract).

Yu, J.J., and Mao, J.W., 2002, 40Ar-39Ar dating of albite in Fe-bearing porphyrite in Ningwu region: Progress in Natural Sciences, v. 12, p. 1059–1063.

Yuan, H.L., Gao, S., Liu, X.M., Liu, H.M., Günther, D., and Wu, F.Y., 2004, Accurate U–Pb age and trace element determinations of zircon by laser ablation inductively coupled plasma mass spectrometry: Geostandard and Geoanalytical Research, v. 28, p. 353–370.

Yuan, H.L., Wu, F.Y., Gao, S., Liu, X.M., Xu, P., and Sun, D.Y., 2003, Determination of U–Pb age and Rare Earth Element Concentrations of Zircons from Cenozoic Intrusions in Northeastern China by Laser Ablation ICP-MS: Chinese Science Bulletin, v. 48, p. 1511–1520.

Zhai, Y.-S., Xiong, Y.-l., Yao, S., and Lin, X., 1996, Metallogeny of copper and iron deposits in the Eastern Yangtze Craton, east-central China: Ore Geology Reviews, v. 11, p. 229–248.

Zhai, Y.S., Yao, S.Z., and Lin, X.D., 1992, Metallogeny of Iron and copper (gold) deposits in the middle-lower reaches of Yangtze River: Beijing, Geological Publishing House, 235 p.

Zhang, Q., Qian, Q., and Wang, Y., 2001a, An east China plateau in mid-late Yanshanian period: implication from adakites: Scientia Geologica Sinica, v. 36, no. 2, p. 248–255, (in Chinese with English abstract).

Zhang, Q., Wang, Y., and Qian, Q., 2001b, The characteristics and tectonic-metallogenic significances of the adakites in Mesozoic period from eastern China: Acta Petrologica Sinica, v. 17, no. 2, p. 236–244.

Zhou, M.F., Yan, D.P., Wang, C.L., Qi, L., and Kennedy, A., 2006, Subduction-related origin of the 750Ma Xuelongbao adakitic complex (Sichuan Province, China): Implications for the tectonic setting of the giant Neoproterozoic magmatic event in South China: Earth and Planetary Science Letters, v. 248, p. 271–285.

Zhou, T., Li, X.M., Zhao, J.S., and Zhang, F.T., 1987, Geochronology of igneous rocks from the Tongguanshan ore area of Anhui Province: Journal of China University of Science & Technology, v. 17, p. 403–407.

Zhou, X.M., and Li, W.X., 2000, Origin of late Mesozoic igneous rocks in southeastern China: Implications for lithosphere subduction and underplating of mafic magmas: Tectonophysics, v. 326, p. 269–287.